



**CALIFORNIA
ENERGY COMMISSION**



**CALIFORNIA
NATURAL
RESOURCES
AGENCY**

**ENERGY RESEARCH AND DEVELOPMENT DIVISION
FINAL PROJECT REPORT**

**High-Resolution Source Mapping to
Minimize Impacts of Waste Biomass
Distributed Generation on Ozone Air
Quality in Disadvantaged Communities
in the San Joaquin Valley**

June 2024 | CEC-500-2024-066



PREPARED BY:

Ling Jin
Yuhan Wang
Sarah Smith
Sarah Nordahl
Tin Ho
Corrine Scown
Lawrence Berkeley National Laboratory
Primary Authors

Agreement Number: EPC-17-028

Joe O'Hagan
Project Manager
California Energy Commission
Energy Research and Development Division

Jonah Steinbuck, Ph.D.
Director
ENERGY RESEARCH AND DEVELOPMENT DIVISION

Drew Bohan
Executive Director

DISCLAIMER

This report was prepared as the result of work sponsored by the California Energy Commission (CEC). It does not necessarily represent the views of the CEC, its employees, or the State of California. The CEC, the State of California, its employees, contractors, and subcontractors make no warranty, express or implied, and assume no legal liability for the information in this report; nor does any party represent that the uses of this information will not infringe upon privately owned rights. This report has not been approved or disapproved by the CEC, nor has the California Energy Commission passed upon the accuracy or adequacy of the information in this report.

ACKNOWLEDGEMENTS

This work was carried out at the Lawrence Berkeley National Laboratory, which is operated for the U.S. Department of Energy under Contract Grant No. DE-AC02-05CH11231. The researchers acknowledge Jeremy Avise at the California Air Resources Board for data sharing, and Lucas Bastien, Wei Zhou, Huy Phan, Quentin Mayemba, and Nancy Brown at Lawrence Berkeley National Laboratory for their assistance in model and data preparation and valuable feedback. The project has benefitted from regularly receiving feedback from technical advisory committee members including David Nunes from the San Joaquin Air Pollution Control District, Wenjun Qian from the California Energy Commission, Lucas Bastien from Atmo Hauts-de-France, and Phil Martien from the Bay Area Air Management District.

PREFACE

The California Energy Commission's (CEC) Energy Research and Development Division supports energy research and development programs to spur innovation in energy efficiency, renewable energy and advanced clean generation, energy-related environmental protection, energy transmission, and distribution and transportation.

In 2012, the Electric Program Investment Charge (EPIC) was established by the California Public Utilities Commission to fund public investments in research to create and advance new energy solutions, foster regional innovation, and bring ideas from the lab to the marketplace. The EPIC Program is funded by California utility customers under the auspices of the California Public Utilities Commission. The CEC and the state's three largest investor-owned utilities—Pacific Gas and Electric Company, San Diego Gas and Electric Company, and Southern California Edison Company—were selected to administer the EPIC funds and advance novel technologies, tools, and strategies that provide benefits to their electric ratepayers.

The CEC is committed to ensuring public participation in its research and development programs that promote greater reliability, lower costs, and increase safety for the California electric ratepayer and include:

- Providing societal benefits.
- Reducing greenhouse gas emission in the electricity sector at the lowest possible cost.
- Supporting California's loading order to meet energy needs first with energy efficiency and demand response, next with renewable energy (distributed generation and utility scale), and finally with clean, conventional electricity supply.
- Supporting low-emission vehicles and transportation.
- Providing economic development.
- Using ratepayer funds efficiently.

For more information about the Energy Research and Development Division, please visit the [CEC's research website \(www.energy.ca.gov/research/\)](http://www.energy.ca.gov/research/) or contact the Energy Research and Development Division at ERDD@energy.ca.gov.

ABSTRACT

Increasing the technical and environmental performance, value, and reliability of waste-to-energy bioenergy systems can facilitate meeting California’s energy and greenhouse-gas emission-reduction mandates. California’s San Joaquin Valley, with its abundant biomass waste streams, has long been out of compliance with the National Ambient Air Quality Standard for ozone, contributing to some of the worst pollution burdens in the state. Understanding how to ease this pollution burden given the planned future scaling up of waste-biomass distributed generation, is critically needed for this region. This project conducts a first-of-its-kind study that quantifies the relative importance of individual-source locations based upon their impacts on existing ozone burdens to disadvantaged communities and ambient air quality non-attainment areas. The key geospatial datasets developed from this project provide quantitative estimates of the ozone impact potential of individual model grid locations. These estimates can enable quick and accurate evaluation of the environmental costs and benefits of waste biomass-to-energy facility deployment strategies and scenarios in the planning stages. The analysis tool and framework developed through this project can be extended in future work to include other criteria pollutants or greenhouse gases in other major air basins in California.

Keywords: ozone pollution burdens, disadvantaged communities, ozone exceedance in the San Joaquin Valley, individual source locations, waste biomass-to-energy facility deployment strategies, spatial and temporal specificity of pollution impact attribution

Please use the following citation for this report:

Jin, Ling, Yuhan Wang, Sarah Smith, Sarah Nordahl, Tin Ho, and Corrine Scown. 2024. *High-Resolution Source Mapping to Minimize Impacts of Waste Biomass Distributed Generation on Ozone Air Quality in Disadvantaged Communities in the San Joaquin Valley*. California Energy Commission. Publication Number: CEC-500-2024-066.

TABLE OF CONTENTS

Executive Summary	1
Introduction	1
Project Approach	1
Project Results	1
Knowledge Transfer and Next Steps	2
CHAPTER 1: Introduction	3
CHAPTER 2: Project Approach	5
Overview	5
CMAQ Forward Simulations.....	5
Study Domain.....	5
Modeling Episodes	6
CMAQ Model.....	8
Input Data	8
CMAQ Adjoint Simulations	9
Adjoint Sensitivity Analysis.....	9
Impact Metric.....	10
CMAQ_adj Model	11
CHAPTER 3: Spatial Heterogeneity in Resulting Impact Potential and its Implications	13
Spatial Heterogeneity in Impact Potential.....	13
Ozone Regime Delineation.....	16
Location-Specific Emission Limit Derivation	19
High-Resolution Benefits	21
Chapter Summary.....	25
CHAPTER 4: Case Study: Ozone Impact Evaluation for BDG Deployment Scenarios.....	26
Introduction	26
Background.....	27
Methodology	28
BDG Deployment Systems	31
Net-Precursor Emissions.....	34
Net Ozone Exceedance Impacts of 32 BDG Scenarios	36
Importance of Facility Siting	38
Chapter Summary.....	39
CHAPTER 5: Conclusions	40
References.....	43
APPENDIX A: Modeling Protocol.....	A-1
APPENDIX B: Emission Factors.....	B-1

LIST OF FIGURES

Figure 1: Modeling Procedure Overview.....	5
Figure 2: SARMAP Modeling Domain Indicated by Purple Rectangle	6
Figure 3: Eight-Hour Ozone Anomalies (ppb) for Three Representative Ozone Episodes, with Arrows Illustrating Featured Flow Patterns (Jin et al., 2013).....	7
Figure 4: Spatial and Temporal Weights of the O _x Burden Receptor	10
Figure 5: Ozone Exceedance in Shaded Areas (Based on Simulated 8-Hour Peak Ozone Concentration Fields)	11
Figure 6: Spatial Distribution of Impact Potential S^+ (X, Y, T) of NO _x Emissions	14
Figure 7: Spatial Distribution of Impact Potential S^+ (X, Y, T) of AVOC Emissions	14
Figure 8: Ozone Regimes Based on Additive Adjoint Sensitivities (S^+)	18
Figure 9: Example of Impact Threshold Specified as the Median of Ozone Impact Attributable to Existing Sources (S^+) Inside the SJV.....	20
Figure 10: Example of Emission Limit Maps Integrated Across Meteorology and Receptors Using 50th Percentile S^+ Impact Thresholds.....	20
Figure 11: Distribution of Derived Emission Limits Compared with Existing Emission Rates at Grid Level in the San Joaquin Valley	21
Figure 12: Example of how Coarse Grids Failed to Capture the Spatial Heterogeneity in Impact Potentials (S^+).....	22
Figure 13: Temporal Patterns of Existing No _x Contributions by Subregion.....	23
Figure 14: Temporal Patterns of Existing AVOC Contributions by Subregion.....	24
Figure 15: Illustration of the Impact Potential and Gridded Emissions Attributable to Source Locations	26
Figure 16: Ozone Exceedance Area in July Episode, Shown in Gray.....	27
Figure 17: Net Emission Calculation Procedure	29
Figure 18: Onsite NO _x Emission Factor of Each Facility Type.....	30
Figure 19: Total Waste Sent to Each Facility in the SARMAP Domain	32
Figure 20: Total Waste in Each Category Sent to SARMAP Facilities	33
Figure 21: Net NO _x Emissions, by Scenario	34
Figure 22: Net VOC Emissions by Scenarios	35
Figure 23: Net Ozone Exceedance Impacts Under 32 BDG-Development Scenarios	36
Figure 24: Generalized Relationships Between Assumptions and Net Impacts, without Consideration of Siting Impacts.....	37

Figure 25: Relationship Between Onsite NO _x Emissions and Their Ozone Exceedance Impacts	38
Figure 26: An Illustrative Example of Siting Importance	39
Figure A-1: Vertical Layer Collapsing Used In This Study	A-3
Figure A-2: Comparison between forward CMAQ_adj and benchmark.....	A-7
Figure A-3: Receptor regions and perturbed emissions domain. Gray rectangle indicates the evaluation subdomain.	A-8
Figure A-4: Relative change in the model response obtained by first-order adjoint sensitivities compared to BF sensitivities method.....	A-9

LIST OF TABLES

Table 1: Definition of Modeling Periods (Based on Jin et al., 2013)	7
Table 2: Definition of Ozone Regimes Based on Additive Adjoint Sensitivities (S ⁺)	16
Table A-1: Species Mapping from SAPRC07 to SAPRC99 (same species are omitted)	A-4
Table A-2: Vertical variation of western BCON for selected species (ppb)	A-6
Table B-1: Emission Factors Used in the Case Study	B-1

Executive Summary

Introduction

Increasing the technical and environmental performance, value, and reliability of waste-to-energy bioenergy systems advance California's ambitious energy and greenhouse gas emission reduction mandates. California's San Joaquin Valley has long been out of compliance with the National Ambient Air Quality Standard for ozone, contributing to some of the worst pollution burdens in the state. Understanding how to ease this pollution burden given the anticipated future scaling up of waste-biomass distributed generation, is therefore critically needed for this region. This project developed a new analytical framework to reduce the air-quality impacts of increasing the utilization of waste biomass in the San Joaquin Valley.

Project Approach

This study applied a high-resolution, state-of-art chemical transport model, coupled to an adjoint tool to quantify the relative importance of individual source locations based on their ozone impacts (quantified by impact potential) on existing ozone burdens in disadvantaged communities and non-attainment areas in the San Joaquin Valley. Adjoint models determine the sensitivity of model outputs with respect to input. The impact potential of a location is defined as receptor-wide ozone impacts from addition of a unit of ozone-forming precursors nitrous oxides, or volatile organic compounds emitted at that location. In this project, two receptors of interest were considered: ozone pollution burdens on disadvantaged communities, and ozone exceedance in the San Joaquin Valley.

Project Results

This project conducted a first-of-its-kind study that quantifies the relative importance of individual source locations based on their impacts on existing ozone burdens to disadvantaged communities and air quality non-attainment areas. The key geospatial datasets developed from this project provide quantitative estimates of the impact potential of individual grid locations. These quantitative impact potential estimates can enable quick and accurate evaluation of environmental costs and benefits of waste biomass-to-energy facility deployment strategies and scenarios in the planning stages. The analysis tool and framework developed through this project can be extended in future work to include other criteria pollutants or greenhouse gas emissions in other major air basins in California.

The research team performed ensemble simulations driven by a range of weather conditions and, separately, for two receptors. The modeling results were used to delineate high- and low-impact locations to determine sizes and emission limits of biomass distributed generation projects and guide decisions on optimal siting and emission control targets for these facilities in a cost-effective and damage-minimizing fashion.

A major highlight of our primary research output — the quantitative estimate of the impact potential of all possible locations — is its ability to enable quick and accurate evaluation of the

environmental costs and benefits of biomass distributed generation deployment strategies and scenarios in the planning stages. These evaluations do not require re-running expensive and time-consuming computer simulations and are additionally much more accurate and robust than previous reduced-complexity tools. This project demonstrates the application of the resulting impact assessment datasets to organic waste management systems under 32 bio-energy development scenarios.

Another salient highlight of the project results is the high resolutions involved in the project's Community Multiscale Air Quality model adjoint (CMAQ_adj) modeling tool, which attributes ozone changes in a receptor region to all possible individual emission sources. This high resolution is either high spatial resolution (4 km × 4 km modeling grids) or high temporal resolution (hourly). The CMAQ adj modeling tool used in this project can therefore provide highly resolved, accurate information on how emission changes at every location affects ozone responses in the San Joaquin Valley. Previous research has never achieved this spatial and temporal specificity of pollution impact attribution because of its high computational cost. Several applications of the resulting high-resolution datasets are demonstrated in this project, including delineation of location specific ozone control priorities and emission limits.

Knowledge Transfer and Next Steps

Over the course of this project, the team shared project results and highlights with a wide range of stakeholders, including regulatory bodies in California (including the San Joaquin Air Pollution Control District, the Bay Area Air Quality Management District, and the California Air Resources Board), as well as experts and researchers both inside and outside of California (during annual meetings of the American Geophysical Union). The team presented at annual meetings of the American Geophysical Union in 2019, 2020, and 2021, and also presented to key experts at the California Energy Commission. The team published two journal articles based on data and analysis that were initially developed from this project (Wang et al., 2022; 2023). The team regularly presented to and received feedback from the technical advisory committee, which included experts from state agencies, California air quality districts, and the research community. To widely demonstrate and share the data products from this project, the project team also developed an interactive display at adjoint.lbl.gov and presented it during technical advisory committee meetings.

Although there have been extensive ozone modeling studies on San Joaquin Valley in the past, this study is the first of its kind and was produced with entirely new information that highlights efficient and cost-effective opportunities that minimize impacts of biomass distributed generation by supporting impact-minimizing site selections and emissions controls. The development of this analytical tool and the framework for prioritizing biomass distributed generation siting together provide several benefits to California. For example, the analysis tool and framework developed through this project can be extended to include other criteria pollutants and greenhouse gases and other major air basins in future emission years.

CHAPTER 1:

Introduction

Waste biomass is an abundant resource in California, and its conversion to energy contributes to the state's ambitious environmental mandate to create 12,000 MW of renewable distributed generation as well as to the goal of diverting 75 percent of organic waste from landfills by 2025. As of 2020, organic waste diversion rates were approximately 42 percent (Paben, 2021). This diverted organic material can provide abundant feedstock for waste biomass distributed generation (BDG). This renewable generation is incentivized by Senate Bill (SB) 1122, which requires that the California Public Utilities Commission (CPUC) direct investor-owned utilities to procure at least 250 MW of power from new, small biopower projects in a separate tariff program. Bioenergy is also an option under community aggregation systems, which allow local communities to choose alternative mixes of "green" energy sources. For all of these reasons, waste biomass is poised to play a major role in California's low-carbon future.

The full potential of BDG, however, will not be reached until air quality impacts can be efficiently and affordably minimized. Air quality concerns are among the key barriers to the growth of this environmental industry. Current bioenergy generation generally involves the combustion of biomass or digester gas and other associated processes, which together produce air pollutants, nitrogen oxides (NO_x), and volatile organic compounds (VOC). These pollutants react in the atmosphere to form ozone, a health-damaging air pollutant that exceeds the health-based national standard in many regions of California.

A recent University of California, Irvine, study (Carreras-Sospedra et al., 2016) showed that bioenergy production at its full potential, under current permitted technologies, could substantially exacerbate ozone air pollution in the San Joaquin Valley (SJV), where disadvantaged communities already suffer from poor air quality. Although air quality impacts from BDG can be mitigated by more advanced technologies and stricter emission controls, across-the-board implementation of these measures can be both expensive and inefficient.

Ozone formation is a complex regional problem. The ozone impact on a community can originate from emissions located far outside of the community region (Jin et al., 2008 and 2011). The contribution to ozone pollution at a given downwind location — such as in disadvantaged communities — also varies by source location depending on wind direction, topography, temperature, and chemical reactions of primary emissions with other atmospheric pollutants. This project developed critical geospatial datasets and tools that can estimate the regional impacts of potential or existing facility sites so that ozone-mitigation strategies can be tailored to location and facility attributes, facilitating widespread deployment of BDG while protecting air quality throughout the state.

This project focused on the SJV area and conducted a first-of-its-kind study to quantify the relative importance of individual source locations according to their ozone impacts (quantified as impact potential) on ozone burdens in both disadvantaged communities and nonattainment areas. The SJV was chosen because it has abundant biomass waste streams and has long

been out of compliance with the national ambient air quality standards (NAAQS) 8-hour standard for ozone. Additionally, it is severely out of attainment with California's 1-hour ambient air quality standard for ozone. The San Joaquin Valley is also the state's most polluted disadvantaged community. Understanding how to mitigate regulatory challenges to ease this pollution burden, given future scaling up of BDG, is especially needed for this region.

This study determined the ozone impact potential of individual locations by the application of a high-resolution, state-of-the-art chemical transport model, coupled with an adjoint tool. The impact potential of a location is defined as the receptor-wide ozone impacts from the addition of a unit of ozone-forming precursors (NO_x or VOC) emitted at that location. In this project, two impact metrics were considered: ozone pollution burdens on disadvantaged communities and ozone exceedance in the SJV.

The research team performed ensemble simulations driven by a range of weather conditions and for two impact metrics. Modeling results delineated high- and low- impact locations to determine the size and emission limits of BDG projects and guide decisions on optimal BDG siting and emission control targets in a cost-effective, minimally damaging fashion. The analysis tool and framework developed in this project can be extended to future work on other criteria pollutants or greenhouse gases, other major air basins in California, and future emissions projections.

The goals of this project were to:

1. Quantify the relative impact of individual existing and potential BDG facility locations in terms of their effects on ozone concentrations in SJV disadvantaged communities as well as meet the federal 8-hr ozone standard of 0.070 parts per million (ppm).
2. Determine location-dependent emission limits for BDG deployment that are both protective of the public health of disadvantaged communities and also meet federal ozone standards.
3. Understand the effects of variable weather conditions on the impact potential of waste-biomass facilities.
4. Provide high-resolution geospatial information to guide damage-minimizing decisions for BDG siting priorities and technology choices.
5. Develop a new analytical framework to assist planners in reducing the air-quality impacts of increasing the utilization of waste biomass throughout California by strategically siting these facilities.

Chapter 2 describes the project's modeling approach. For technical details, more information about model calibration, evaluation, and datasets can be found in Appendix A. Chapter 3 describes the primary outputs from project production runs (the impact potential maps of existing and potential source locations) and discusses their multiple applications for optimizing BDG deployment. Chapter 4 demonstrates a detailed application case where impact potential maps were used for fast evaluation of ozone impacts from 32 BDG deployment scenarios. The importance of facility siting is also illustrated. Chapter 5 concludes the findings with project contributions and impacts.

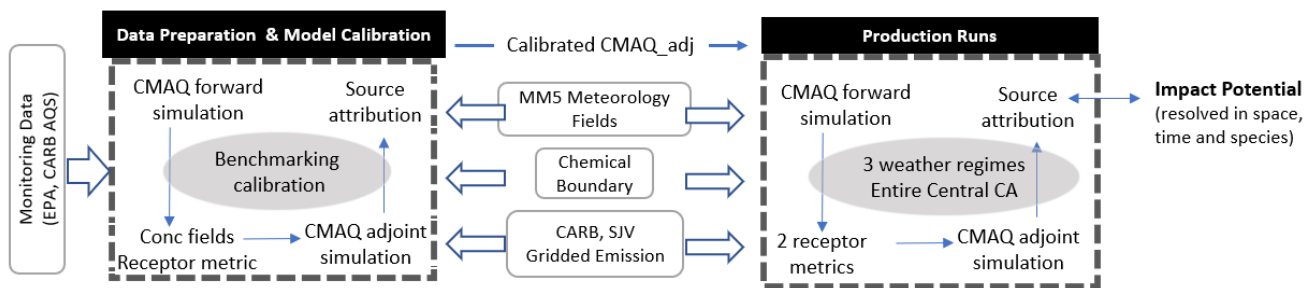
CHAPTER 2: Project Approach

Overview

This chapter summarizes the modeling procedure conducted in this study. Figure 1 is an overview of the modeling procedure. Additional technical details can be found in Appendix A. The primary goal of these simulations is to attribute ozone impact to individual source locations. The impact potential attributed to a location is defined as receptor-wide ozone impacts from addition of a unit of ozone-forming precursors emitted at that location.

The project team used the adjoint of Community Multiscale Air Quality modeling system (CMAQ adj) as the modeling tool and performed three main steps in production runs: CMAQ forward simulations, defining impact metrics of interest, and CMAQ adjoint simulations.

Figure 1: Modeling Procedure Overview



In CMAQ forward simulations, ozone pollution was simulated under three meteorologically representative high-ozone episodes. Based on forward simulation outputs, two impact metrics of interest were defined, representing: ozone pollution burdens on SJV disadvantaged communities, and ozone exceedance in the SJV. Finally, taking both forward-run outputs and impact metrics as inputs, backward simulations (or adjoint sensitivity analyses) were performed in the CMAQ_adj system.

Descriptions about each step and an overview of primary model outputs are provided in the following sections.

CMAQ Forward Simulations

Study Domain

The study domain is a sub-region (34.5° to 39°N and 118.5° to 123°W) of the domain selected for the Central California Ozone Study, which consists of several geographically divided air basins shown in Figure 2, including the SJV air basin and its major upwind-source regions.

The San Joaquin Valley is surrounded by the Sierra Nevada and coastal ranges. On typical summer days, westerly winds are funneled into the Central Valley through gaps in coastal

ranges, with large portions of the flow directed into SJV. The San Francisco Bay Area and the Sacramento Valley are therefore the major upwind SJV emission sources. Two busy highways run through the SJV: Highway 99 connects the major urban centers, and Interstate 5 runs through rural and agricultural areas. Air basins are labeled on the map for the San Francisco Bay Area (SFB), Sacramento Valley (SV), mountain counties (MC), San Joaquin Valley (SJV), North Central Coast (NCC), and South Central Coast (SCC).

The study domain (SJVAQS/AUSPEX Regional Modeling Adaptation Project [SARMAP] domain) was modeled with a horizontal resolution of 4 km. Vertically, the domain was divided into 35 layers from the surface to 100 mb (about 17 km), and the near-surface layers were about 20 m thick. The model used a terrain-following vertical coordinate system.

Figure 2: SARMAP Modeling Domain Indicated by Purple Rectangle



Modeling Episodes

Three ozone episodes were selected from a cluster analysis that identified representative meteorological regimes in the SJV modeling domain (Jin et al., 2013). Each episode was named after the region where ozone (O_3) concentrations were high during the period: O_3 -All, O_3 -South, and O_3 -West (Jin et al., 2013, Figure 3). For example, from July 29th to August 2nd, O_3 is high throughout the valley. These episodes were extended to 7-day modeling periods (Table 1), which included a 4-day model spin-up at the beginning of each period. Forward simulations show that these three episodes (O_3 -All, O_3 -South, O_3 -West) are associated with ozone exceedance in the SJV so were therefore considered for the adjoint runs.

Figure 3: Eight-Hour Ozone Anomalies (ppb) for Three Representative Ozone Episodes, with Arrows Illustrating Featured Flow Patterns (Jin et al., 2013)

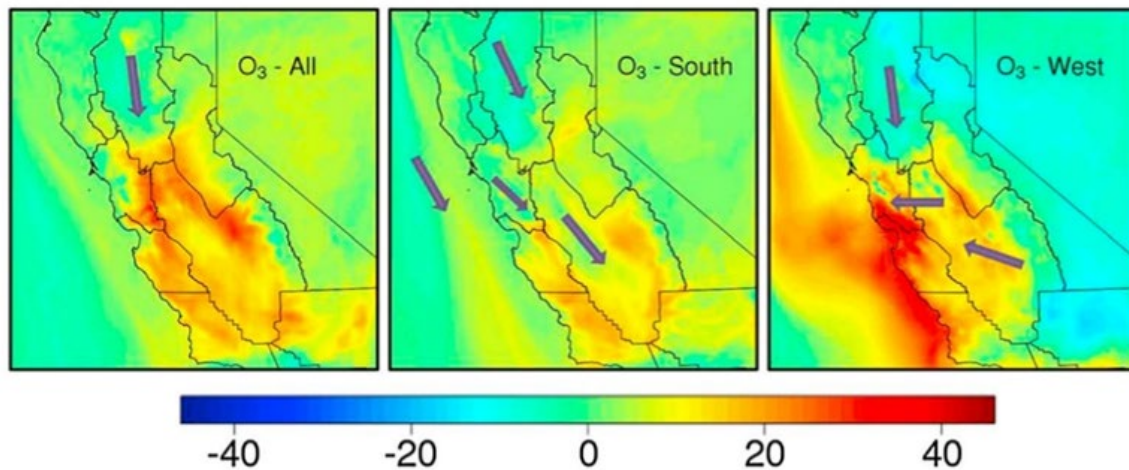


Table 1: Definition of Modeling Periods (Based on Jin et al., 2013)

Condition Categories	Modeling Periods	Ozone Episode
O₃-All (Jul)	July 27 to August 2 (days 209 – 215)	July 29 to August 2
O₃-South (Aug)	August 11 to 17 (days 224 - 230)	August 14 to 17
O₃-West (Sept)	September 14 to 20 (days 258 -264)	September 17 to 20

Although these episodes were sometimes referred to as “July/August/September episodes” according to their modeling periods, they are not monthly averages. These episodes instead represent distinct ozone-inducing meteorology regimes, each resulting in different spatial patterns of elevated ozone concentrations. Since SJV meteorology regime types were quite stable across years, our modeling results are not year-specific, but more generalized in the context of different years.

The **July (O₃-All)** episode is associated with a persistent “Western U.S. High” system with high temperatures and light winds. Its flow patterns resemble the summer mean. Pollutant concentrations are elevated in much of the SJV.

The **August (O₃-South)** episode is under the influence of a Western U.S. High anticyclone system located inland, which leads to higher temperatures in the eastern and southern part of the domain. The temperature-induced pressure gradient enhances the down-valley and upslope ventilation flows, increasing pollutant levels in the southeastern part of the SJV.

The **September (O₃-West)** episode is the most stagnant episode among them, under the influence of an “Eastern Pacific High” system. Under this meteorology regime, the ocean and coastal areas are heated up, leading to weakened onshore flows from west (ocean) to east (land). Pollutant concentrations thus tend to increase on the western side of the SJV.

CMAQ Model

Community Multiscale Air Quality (CMAQ) Version 4.5 is the chemical transport modeling system used in this study, where ozone performance has been extensively evaluated and benchmarked for this domain (Jin et al., 2007, 2010). CMAQ is developed by the United States Environmental Protection Agency (U.S. EPA) and consists of three primary components: meteorology, emissions, and a chemical transport model (along with several interface processors). This model accommodates many different science-process modules that provide one-atmosphere and community multiscale modeling capability (Byun and Schere, 2006).

In this project CMAQv4.5, or the forward model, was calibrated for the SJV domain. It was configured to use the piecewise parabolic method for advection, multiscale horizontal diffusion, and eddy vertical diffusion (Hakami et al., 2007) (same as Jin et al., 2008 and 2010). The forward model was evaluated by conducting a 5-day simulation then comparing a simulated 8-hour peak ozone against previous benchmark simulations (in Jin et al., 2008), for the same domain and exhibit satisfactory agreement (for details see Appendix A, Figure A-2).

Configuration options were mostly based on past ozone modeling studies for the SJV domain, except for the choice of vertical layers. Previous studies used mostly 18 or 27 vertical layers. Although the team did find that layer-collapsing choices have minimal effects on the forward-run results, later backward simulations required a more cautious decision on vertical layers; 27-layer backward simulation returned errors such as unreasonably huge sensitivities, so after a few diagnostic runs researchers ultimately used 35 vertical layers for both forward and backward runs.

Input Data

Four categories of data were prepared as inputs for air-quality modeling in this study: meteorological inputs, gridded emission profiles, lateral chemical boundaries, and initial conditions.

Meteorological Inputs with 4 km resolution were simulated by Wilczak and co-workers at the National Oceanic and Atmospheric Administration (NOAA) (<http://www.etl.noaa.gov/programs/modeling/ccos/>), using the National Center for Atmospheric Research/Pennsylvania State University Mesoscale Meteorological Model Version 5 (MM5) (Grell et al., 1994) Version 3 for a historical summer season starting at 1,200 Coordinated Universal Time (UTC) June 1 to 1,200 UTC September 30, 2000. The Meteorology to Chemistry Interface Processor (MCIP Version 3.6) was used to construct CMAQ model-ready input files from the MM5 output and allowed the consolidation of vertical layers. The team used 35 layers for CMAQ from the original 50 MM5 layers without changing the first 1600 m (28 layers) to preserve high resolution within the planetary boundary layer (PBL).

Gridded Emission Profiles of gaseous species were derived from the 2012 Emission Inventory for the SJV Ozone State Implementation Plan at the time of this study (SJVAPCD, 2016), prepared by the California Air Resources Board (CARB). The gridded emissions are provided in two types of files: one is the merged emissions including anthropogenic (point, area, and mobile sources) and biogenic sources, and the other is the biogenic emissions only. The SARMAP domain (96 by 117) is contained within the CARB domain, with the same horizontal resolution and map projection. The anthropogenic portion of the CARB emission data is

originally speciated under the Statewide Air Pollution Research Center (SAPRC) SAPRC07 chemical mechanism (Carter, 2010a) and is mapped to the SAPRC99 speciation (Carter, 2000) required for CMAQv4.5. SAPRC99, including 72 chemical species and 211 reactions. Because the Year 2000 meteorological inputs are used to drive the chemical transport model, and variations in biogenic emissions are largely driven by light and temperature fields, 2012 anthropogenic emissions were merged with the meteorologically driven biogenic emissions of Year 2000 (documented in Jin et al., 2010).

Lateral Chemical Boundary Conditions (BCON) define the chemical species mixing ratio at the four boundaries at which air enters or leaves the modeling domain. Vertically varying boundary conditions are provided by CARB at hourly resolutions; CARB BCON was derived from global simulations, using the Model for Ozone And Related Chemical Tracers (MOZART) Version 4 (Emmons et al., 2010). As the CARB BCON is converged under the SAPRC07 chemical mechanisms, mapping to the SAPRC99 mechanism is conducted (see APPENDIX A, Table A-1, for details). The temporal average concentrations of the CARB BCON at each of the four boundaries over the 4-episode time periods represented the chemical environment at the lateral boundaries surrounding the domain.

Initial Chemical Conditions (ICON) defined the mixing ratios of gaseous species in the modeling domain at the beginning of the model simulation. A 4-day spin-up run prior to each episode was used to obtain model initial conditions.

CMAQ Adjoint Simulations

Adjoint Sensitivity Analysis

In the context of air-quality modeling, sensitivity analysis plays a pivotal role in determining the causes and consequences of air pollution. Sensitivity analysis techniques therefore included two broad categories: forward (source-oriented) and backward (receptor-oriented) techniques.

A majority of the sensitivity analyses fall into the forward category, including but not limited to the brute-force method, complex-step approach, and the decoupled-direct method. These forward techniques efficiently calculate sensitivities of all model outputs with respect to one single-input perturbation (for example, a region-wide emission perturbation or an emissions change at one specific location).

Complementary to traditional techniques, *adjoint sensitivity analysis* is the only member in the backward family and excels in the opposite situation. This newer method is well suited in cases where there is interest in the response of one specific air-quality metric to the perturbations in every model input. The adjoint method generates sensitivity apportionment fields, which reveal when and where model data are important to the target response (Martien et al., 2006). In other words, the adjoint method can link emission changes at any location and time, with specific contributions to the impact metric of interest. The mathematical formulation of adjoint sensitivity analysis appears in APPENDIX A.

Impact Metric

As discussed previously, the adjoint sensitivity analysis impact metrics should be defined before adjoint (backward) simulations. An impact metric, R , is a user-defined function that represents air-quality impacts of interest.

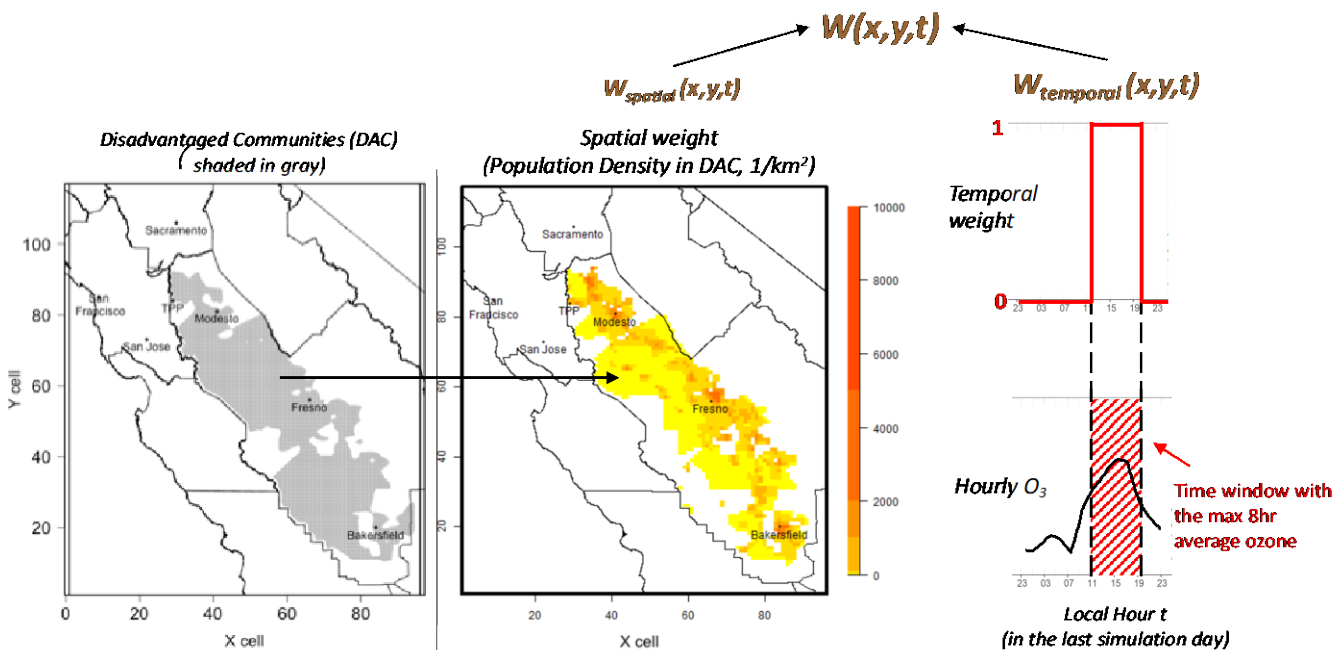
In this study, the team designed two impact metrics, each representing one of two overall goals: protecting SJV's low-income communities from ozone pollution and achieving ozone non-exceedance.

Impact Metric 1: Odd Oxygen Burdens in Disadvantaged Communities

The first impact metric (referred to as *DAC O_x burden*) was designed as population-weighted surface odd oxygen ($O_x = O_3 + NO_2$) concentrations during 8-hour peak ozone hours in SJV disadvantaged communities. The odd oxygen family of chemical compounds comprises ozone and other species with which ozone rapidly cycles and is used as a proxy in this research for ozone-related, air-quality burdens."

Disadvantaged California communities, as defined by the California Environmental Protection Agency (CalEPA) are the top 25 percent of CalEnviroScreen3.0 scoring areas, along with other areas with high levels of pollution and low population. A majority of SJV communities were selected as receptor regions (Figure 4). Odd oxygen ($O_x = O_3 + NO_2$) is considered the pollutant concentration of interest in this impact metric. Since O_3 and NO_2 can rapidly interconvert in the presence of sunlight and both have adverse health effects, odd oxygen is considered a better indicator of the net photochemical production of O_3 and its associated health burdens on residents.

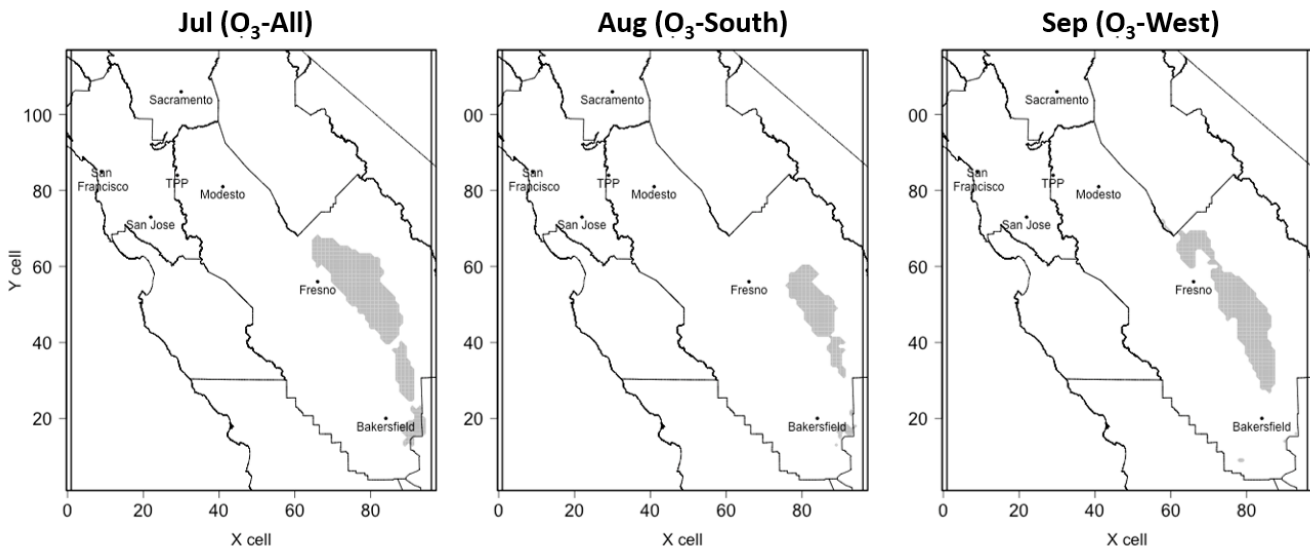
Figure 4: Spatial and Temporal Weights of the O_x Burden Receptor



Impact Metric 2: Ozone Exceedance

The second impact metric (referred to here as *ozone exceedance*) identifies 8-hour peak ozone concentrations in exceedance areas in the SJV. The ozone exceedance areas are locations where 8-hour peak ozone concentrations in forward-run outputs exceed the NAAQS of 70 parts per billion (ppb). The shaded areas in Figure 5 show ozone exceedance areas under each of the three modeling scenarios.

Figure 5: Ozone Exceedance in Shaded Areas (Based on Simulated 8-Hour Peak Ozone Concentration Fields)



CMAQ_adj Model

To perform adjoint (backward) simulations, the team used the adjoint code coupled with CMAQ (CMAQ_adj), which was originally developed by Hakami et al., 2007, with modification from Bastien et al., 2015, which used the SAPRC99 chemical mechanism with ROSENBROCK chemical solver instead of the original CB-IV chemical mechanism used in Hakami et al., 2007. SAPRC99 includes 72 model chemical species and 211 chemical reactions (listed in Carter, 2000). Moreover, the original code is modified to force the time step for operator splitting (the synchronization time step, [STS]) to be constant throughout the simulation. The same STS is used for both the forward and corresponding adjoint calculations but can vary across simulation periods.

The adjoint code was configured with the same build options as the stand-alone CMAQv4.5 forward model, including chemical mechanisms, advection and diffusion schemes, and horizontal and vertical resolutions. Forward-run inputs and outputs were both used as inputs to adjoint simulations. The accuracy of backward adjoint model was evaluated by comparing adjoint sensitivities with sensitivities obtained by the brute-force (BF) method, in a smaller domain within the SJV. Adjoint and BF show good agreement for perturbations in NO and VOCs with a coefficient of determination $R^2=0.96$. The correlation is about the same if only VOCs are concerned ($R^2=0.96$) (for more detail see Appendix A).

Primary outputs of our production runs are the impact potential, or additive adjoint sensitivities (S^+) resolved in space and time. The additive adjoint sensitivities $S^+(x,y,t)$ represent the sensitivity of the impact metric R to adding (or decreasing) emissions at location (x,y) and time t . Therefore, $S^+(x,y,t)$ represents the impact potential, and indicates the source importance of emission changes at each location and time with respect to a given impact metric. $S^+(x,y,t)$ can be nonzero where and when there are no emissions. When the impact potential is multiplied with the actual emissions occurring at the location and time, the team determined the actual impact of a given emission source, which is expressed as S^+ .

CHAPTER 3:

Spatial Heterogeneity in Resulting Impact Potential and its Implications

The primary outputs of production runs (the impact-potential maps) can be used to support regulatory decision-making in multiple ways. This chapter discusses the spatial heterogeneity in location-specific impact potentials simulated by the adjoint tool, and its direct implications for optimizing ozone-control strategies. Chapter 4 presents a detailed case study that illustrates how the impact-potential map can be used to perform fast-impact evaluations for various BDG deployment scenarios.

Spatial Heterogeneity in Impact Potential

The impact potential for a grid location represents its contribution to the impact metrics by adding a unit of emissions to this location. Figure 6 and Figure 7 present impact potential (S^+) maps with respect to NO_x and anthropogenic volatile organic compounds (AVOC) emission sources, respectively, under three modeling episodes and two impact metrics. An interactive display of the modeling results is provided at: <https://adjoint.lbl.gov/>.

The maps shown here serve as screening tools to inform the siting of future sources. Deeper-red values indicate source locations of greater contribution to the impact metrics.

The maps also indicate that, in most SJV locations, impact potentials of NO_x are higher than those of AVOC for both impact metrics considered. That generally suggests that NO_x emission-control actions are still more important than AVOC-control actions, either for reducing ozone burdens of disadvantaged communities or for achieving ozone attainment. It is consistent with 2016 summer in-situ aircraft data collected in the SJV, which suggested that ozone chemistry was predominantly NO_x -limited in the SJV on sample days (Trousdel et al., 2019).

The magnitude and spatial distribution of ozone impact potentials are greatly driven by impact metric selection. For reducing DAC O_x burdens, both NO_x and AVOC impact potential hotspots (colored in deep red) are mainly found in Northern SJV or upwind regions such as the SFB, Sacramento Valley (SV), and Mountain Counties (MC), depending on meteorology. This finding highlights the importance of regionally coordinated emission control efforts involving not only the SJV but also its upwind areas, for protecting SJV's disadvantaged communities. Since S^+ hotspots are sparsely located inside the valley, by strategically avoiding these hotspots or even relocating existing sources to lower S^+ areas, it is possible to both reach the full potential of biomass distributed generation (BDG) and also protect air quality in disadvantaged communities.

Figure 6: Spatial Distribution of Impact Potential S^+ (X, Y, T) of NO_x Emissions

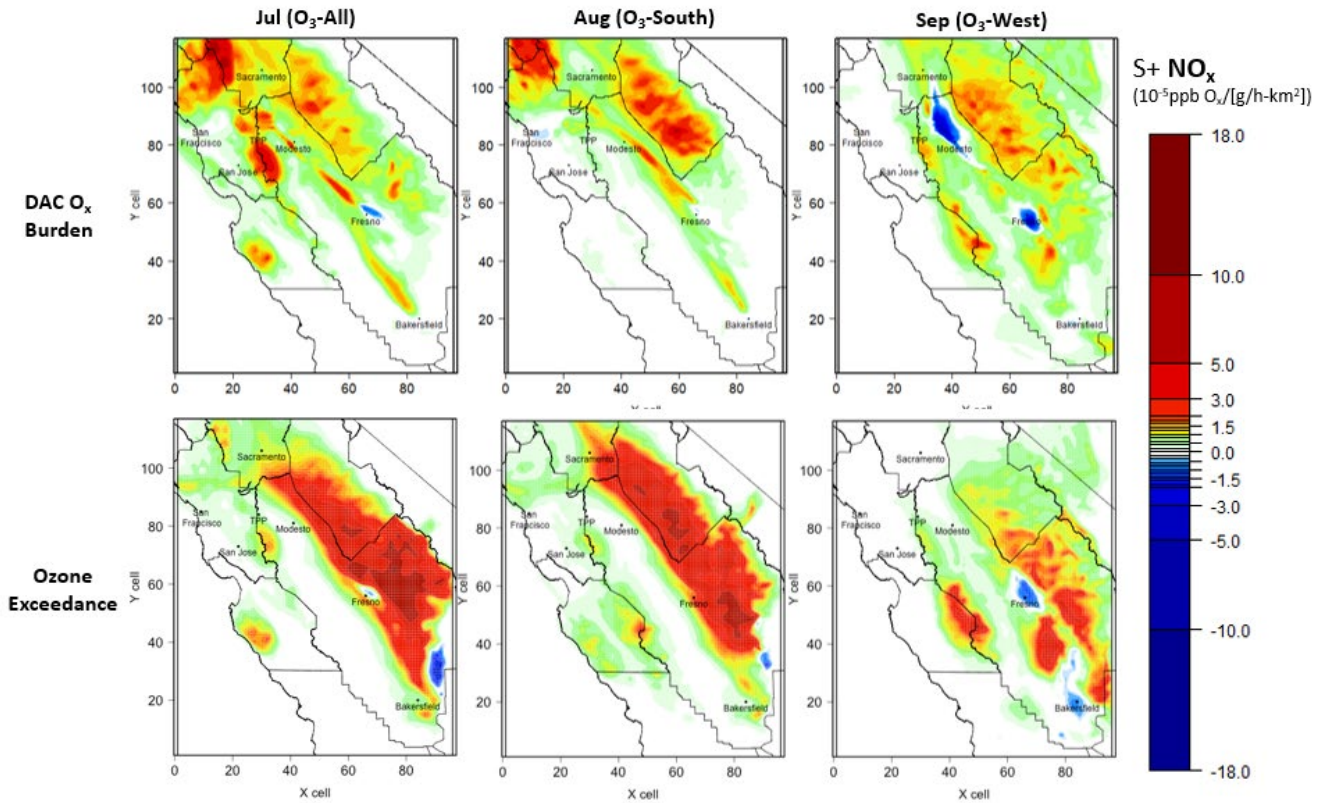
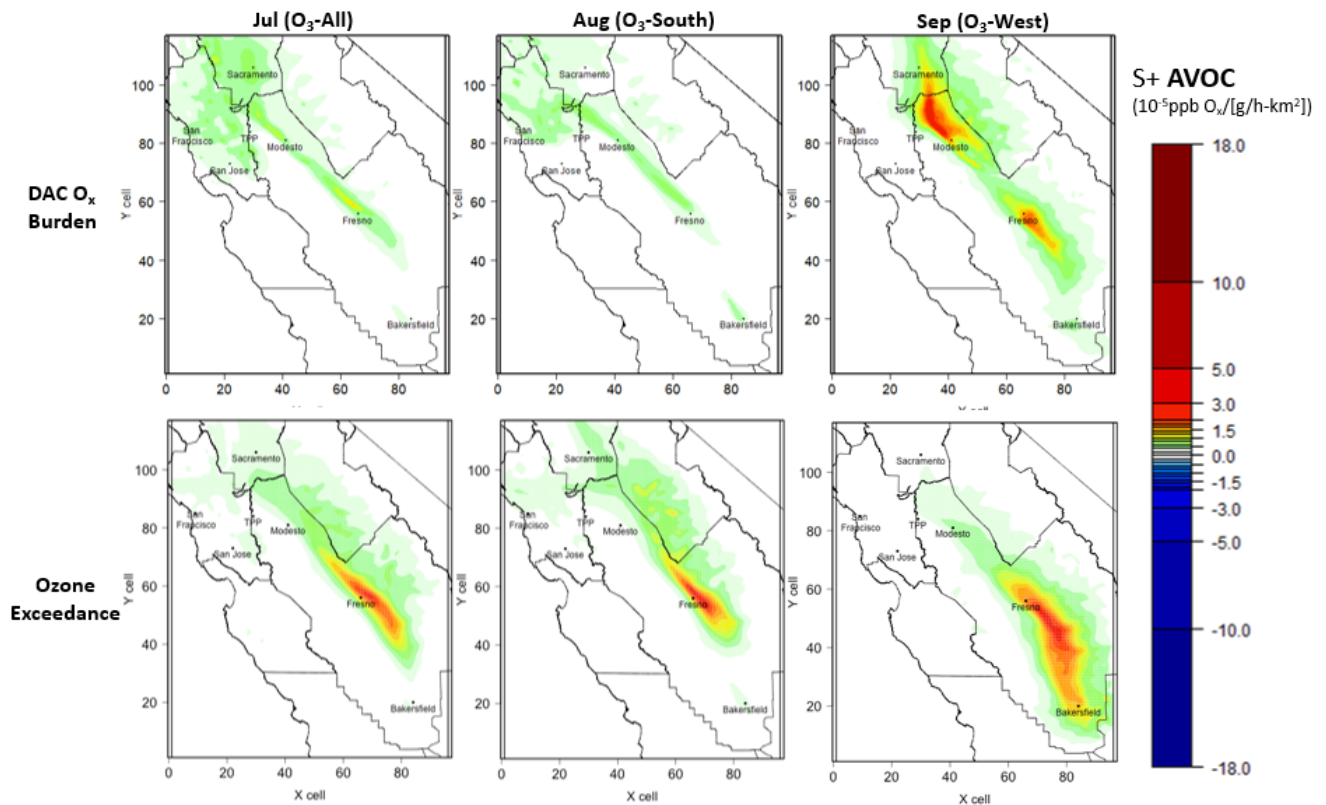


Figure 7: Spatial Distribution of Impact Potential S^+ (X, Y, T) of AVOC Emissions



For meeting federal ozone standards, upwind regions show much lower impact potentials for both NO_x and AVOC. Ozone exceedance areas are typically located in Southeastern SJV in the intermediate downwind of Fresno (and sometimes Bakersfield) emissions. The air masses transported from these urban emission centers are therefore rich in NO_x, which makes AVOC quite impactful. That explains why AVOC emissions — especially those in middle SJV areas around Fresno — tend to show high-impact potential on ozone exceedance under all three meteorological regimes. Meanwhile, because the eastern side of the valley and mountain counties are adjacent to the exceedance area and have rich biogenic volatile organic compounds (BVOC) emissions, NO_x emissions in these regions will also exert significant pressure on ozone exceedance.

For the two different impact metrics, meanings of a negative NO_x S^+ (NO_x disbenefit area, colored in blue) are also different. For the ozone exceedance receptor, NO_x disbenefits can be mainly explained by NO_x titration effects that the reaction $O_3 + NO \rightarrow NO_2 + O_2$ reduces ozone levels. But for the DAC O_x burden receptor, which focuses on odd oxygen ($O_x = O_3 + NO_2$), titration effects ($O_3 + NO \rightarrow NO_2 + O_2$) will not affect O_x levels. Instead, a negative O_x sensitivity to NO_x is associated with the chain termination reaction $OH + NO_2 \rightarrow HNO_3$. In this reaction, adding NO_x emissions promotes the removal of both hydroxyl radicals (OH) and NO_x from the system, resulting in an O_x decrease. We used O_x instead of O₃ as the receptor species because both NO₂ and O₃ have adverse health effects and they can rapidly interconvert with the presence of sunlight; O_x is thus a better indicator to represent the net photochemical production of O₃ and associated health burdens on disadvantaged communities.

The spatial extent of such NO_x disbenefits areas is largely influenced by meteorological conditions. The July (O₃-All) episode features summer mean flow patterns from north to south, with high temperatures. The August (O₃-South) episode shares some similarities but has more enhanced down-valley flows under the influence of a Western U.S. high-anticyclone system located inland. Both episodes have relatively small NO_x disbenefit areas when compared with the most stagnant September (O₃-West) episode with weakened onshore flows (Jin et al., 2013). In the September (O₃-West) episode, due to its great stagnancy, intra-valley emissions will become more influential; the largest NO_x disbenefit areas were mostly around the urban centers of Modesto, Fresno, Bakersfield, and their respective surrounding suburban areas. The explanation to this pattern is that the accumulation of NO_x under stagnant conditions can promote the chain termination reaction $OH + NO_2 \rightarrow HNO_3$, remove OH radicals from the system, and thus shift ozone chemistry more towards VOC-limited. In these urban locations, the importance of AVOC-control increases under this stagnant September (O₃-West) episode.

The September (O₃-West) episode result is of our particular interest. Though this episode is labeled "September," it does not represent the month's average meteorology. Instead, it is a representative meteorological regime (identified in a cluster analysis by Jin et al., 2011) under the impact of an Eastern Pacific High system that heats up the ocean and coastal areas. Induced by the temperature anomaly, an enhanced surface pressure from land to sea (a northeasterly wind anomaly) weakens onshore flows and leads to very stagnant conditions. This meteorology regime is particularly meaningful for two reasons.

It shares great similarities with the meteorological conditions that can increase wildfire occurrences. A recent study systematically investigated 1,535 wildfires in California during 1984-2017 found that the strong northeasterly wind anomaly from inland to the coast, and high surface pressure tends to induce hot, dry conditions favorable for wildfires (Dong et al., 2021). It is consistent with an earlier study that showed that strong northerly and northeasterly winds blowing dry inland air contributed to drought conditions and wildfires in California in October 2017. Considering the fire-prone nature of its meteorology, impact potentials under the September episode can be useful for understanding the ozone impacts of fire-related emission changes.

Secondly, studies have projected that, under the impacts of climate change, California’s SJV will experience more and stronger stagnation events (Zhao et al., 2011b, 2011a). In other words, we can expect that the stagnant meteorological conditions under the September episode will be more frequent in the future. Without effective pollution control actions, the higher occurrence of ozone-inducing meteorology regimes will most likely lead to increased air pollution problems in the region. To mitigate these impacts, it is essential to understand how meteorology will shift impact potentials at each location and adopt strategies accordingly. That is another benefit of this research product. The team provided episode-specific impact potential (S^+) maps, so that decision makers could see meteorological impacts directly and have the flexibility to use individual S+ maps to prioritize the meteorology (or receptor) of most concern.

The project also found that weak correlations ($R^2 < 0.4$) between S^+ and existing emissions were found across receptor, episode, area (SFB, SV, SJV) and precursor type (NO_x , VOC). This consistent weak correlation indicates that location-specific impact potentials are more driven by factors other than by existing emissions. It highlights the necessity and importance of strategic siting decisions for new sources. This finding also supports the usefulness of our impact-potential maps as a screening tool since it can be expected to remain a reasonable estimation for a considerable period of time provided that emission changes are not too abrupt.

Ozone Regime Delineation

Based on the impact potential maps, ozone regimes can be delineated, as defined by the relationship between $NO_x S^+$ and $AVOC S^+$ in Table 2 (Jin et al., 2013, 2008).

Table 2: Definition of Ozone Regimes Based on Additive Adjoint Sensitivities (S^+)

Condition	Regime
$NO_x S^+ > AVOC S^+ > 0$	NOx-limited
$AVOC S^+ > NO_x S^+ > 0$	Transition
$NO_x S^+ < 0$	VOC-limited

Distinct from ozone regimes identified by traditional (forward) sensitivity analysis that describes local chemistry, here the ozone regime map (Figure 8), as identified by adjoint sensitivity analysis) reflects local-emission receptor-wide impacts, including both local and downwind sites within the receptor region. It can be understood as the *optimal ozone control option*

at each location, and thus providing direct guidance for location-specific emission control strategy designs.

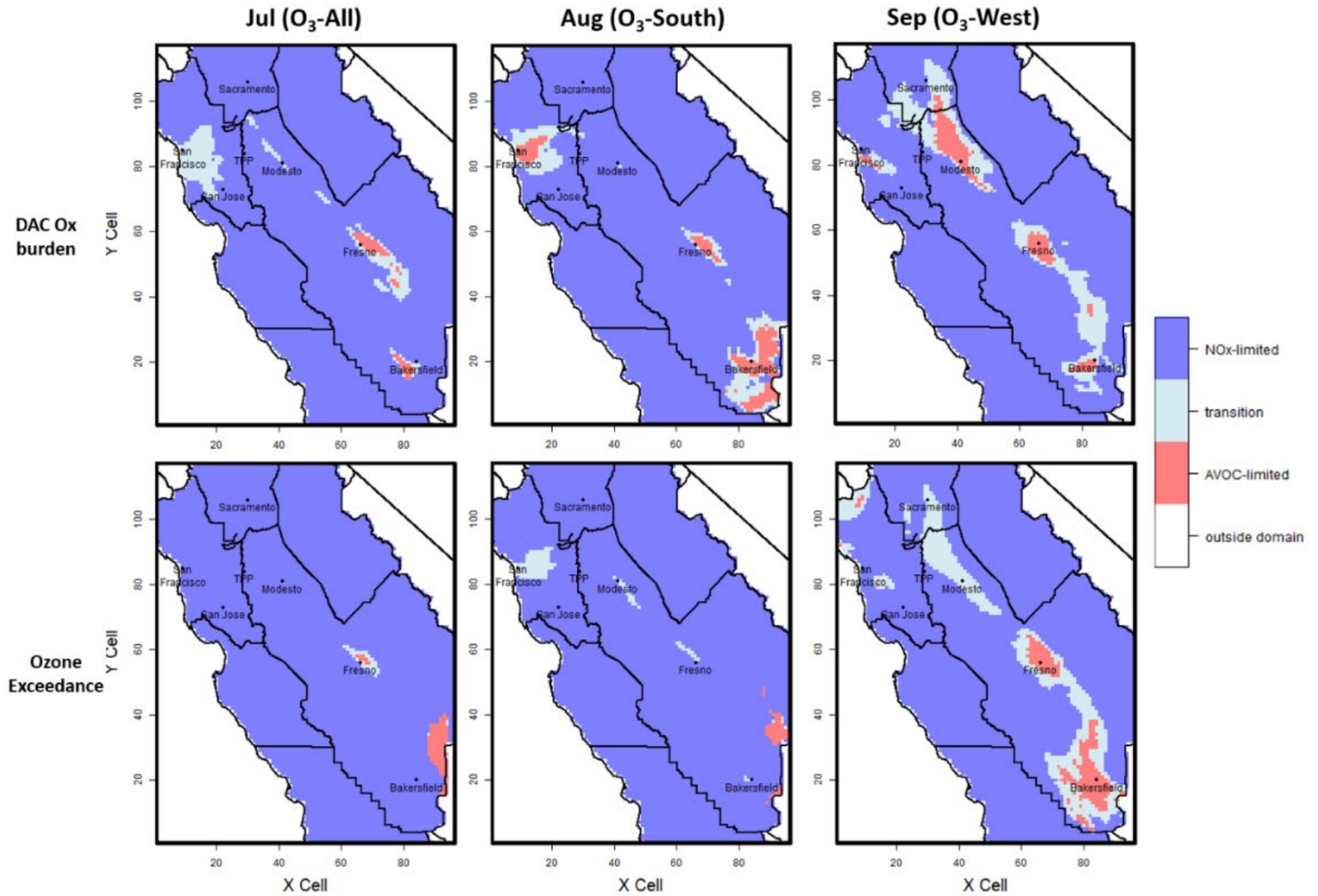
Taking Modesto as an example, under the July (O_3 -All) episode meteorology, it was identified as VOC-limited in a previous study that used forward-sensitivity analysis (Jin et al., 2013). However, based on the impact potential maps developed in this project, Modesto is now NO_x -limited under the same meteorology, which better reflects the optimal ozone control option at this location. Although Modesto NO_x emissions may reduce local ozone levels through titration effects ($O_3 + NO \rightarrow NO_2 + O_2$), the NO_x emitted at Modesto can be transported to enhance ozone formation downwind and increase overall disadvantaged community burdens and ozone exceedance. That said, NO_x control at Modesto is still both necessary and efficient. Such information can only be available through the adjoint (backward) sensitivity analysis technique used in this study. The ozone regime map (Figure 9) is straightforward for decision makers to use for optimizing location-specific ozone control strategies.

In most SJV locations, the optimal ozone control option was identified as NO_x control, either for reducing DAC O_x burdens or reducing ozone exceedance. The spatial extent of VOC-limited areas (areas where AVOC control is more effective than NO_x control) is affected by meteorology or the impact metric of interest.

In Northern SJV, the ozone regime is quite sensitive to meteorology. In days with windy conditions like the July and August episodes, the whole Northern SJV area is predominantly NO_x -limited for both receptors. But under the stagnant September (O_3 -West) episode with weakened onshore flows, Northern SJV will be shifted towards a *VOC-limited* regime, indicating the increased importance of AVOC control, especially for the DAC O_x burden receptor.

The ozone regime in SFB, on the contrary, is more driven by the receptor than meteorology. For reducing SJV ozone exceedance, NO_x control is always more beneficial than VOC control in the SFB area. However, for protecting SJV disadvantaged communities, the relative importance of VOC control in SFB rises, especially in the August (O_3 -South) episode when down-valley winds are enhanced by a Western U.S. High anticyclone system, located inland.

Figure 8: Ozone Regimes Based on Additive Adjoint Sensitivities (S^+)



As for the southern end of the valley, pollutants tend to accumulate due to SJV's unique trough-like topography. The relative importance of NO_x, versus AVOC control at these locations, depends on both meteorology and impact metrics. For the ozone exceedance receptor, the spatial extent of VOC-limited areas in Southern SJV is the most widespread under stagnant conditions (for example, the September episode). For the DAC O_x burden receptor, meteorology impacts on location-specific ozone-control options are less significant and VOC-limited areas were mainly around Fresno and Bakersfield.

The transition between a NO_x-limited ozone regime and a VOC-limited ozone regime is typically found in suburban areas near urban centers (in this case SFB, Modesto, Fresno, and Bakersfield). Its range can extend to some rural areas under the most stagnant September episodes.

Location-Specific Emission Limit Derivation

Another important application of impact potential results is to determine location-dependent emission limits (for BDG deployment or other potential emission sources). For any given impact threshold, the project delineates emission limits at each location throughout the whole modeling domain, based on the relationship:

$$\text{Emission limit} = \frac{\text{impact threshold}}{\text{impact potential } (S^+)} \quad (1)$$

As an example, the team focused on emission limits inside the valley and specified the impact threshold as the median of positive S^x (generated by multiplying impact potential S⁺ map with a Year 2012 gridded emission profile) values inside the valley. Researchers assumed that new sources would be less polluting (as evaluated by sensitivity of impact metrics) than at least half of Year 2012 existing sources in the SJV (Figure 9). This is not a recommended threshold, but rather an example value that illustrates the application. Theoretically, impact thresholds can be any values of interest, depending upon regulatory purposes.

With this example, impact-threshold and emission-limit maps can be derived for each receptor (impact metric) and episode and combined to derive an integrated emission-limit map (Figure 10), which shows the most stringent emission limit at each location for both protecting disadvantaged communities and reducing ozone exceedance. Emission-limit maps are provided at 4-km resolution, enabling a location-dependent emission standard tailored to local conditions.

Figure 9: Example of Impact Threshold Specified as the Median of Ozone Impact Attributable to Existing Sources (S^+) Inside the SJV

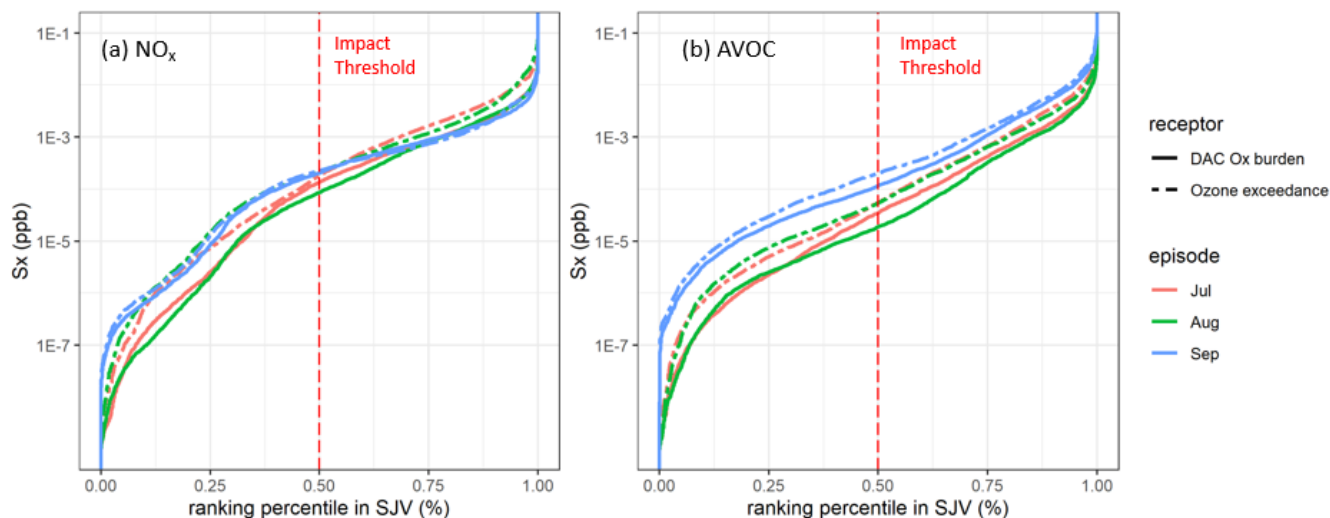
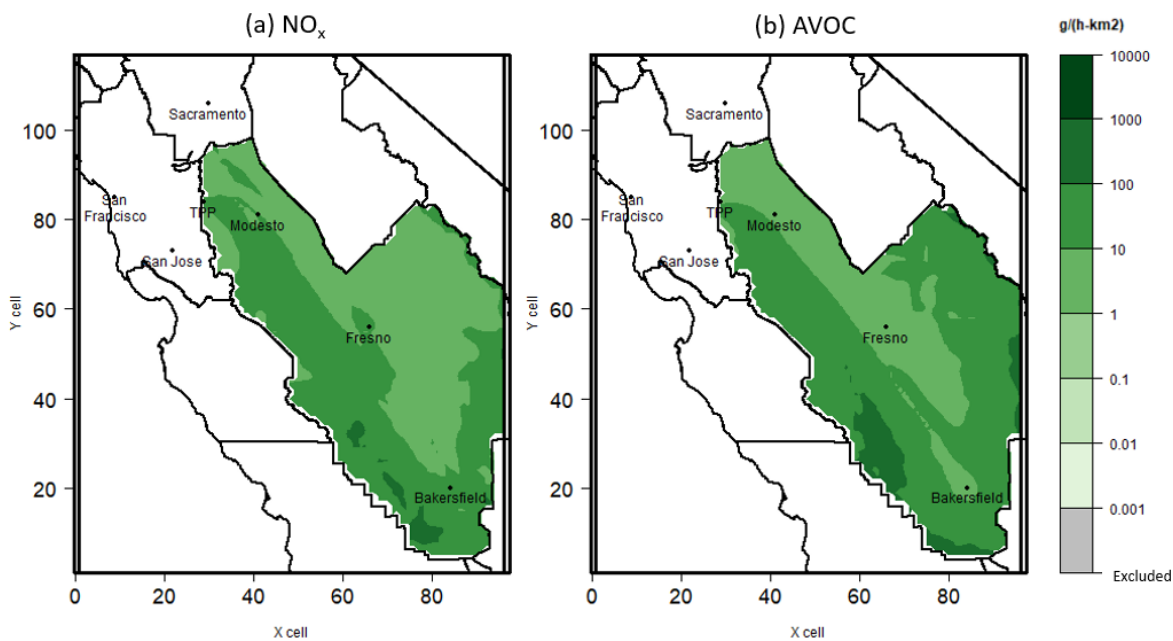
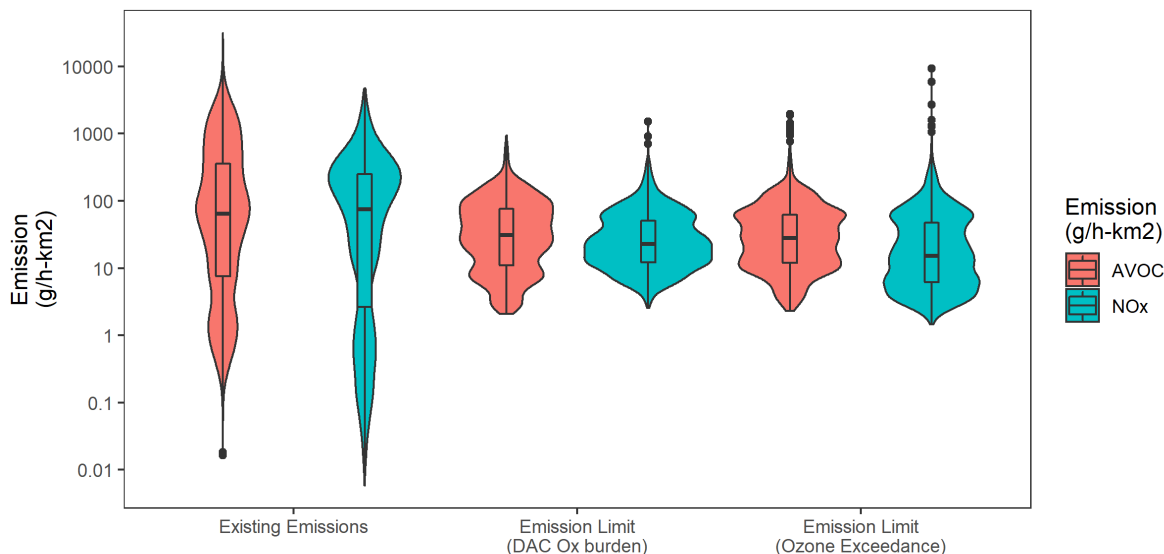


Figure 10: Example of Emission Limit Maps Integrated Across Meteorology and Receptors Using 50th Percentile S^+ Impact Thresholds



The Northern SJV and Bakersfield areas require more stringent emission limits ($<10 \text{ g}/(\text{h}\cdot\text{km}^2)$), while emission limits in the southern and western SJV areas can be looser (up to $100\text{-}1000 \text{ g}/(\text{h}\cdot\text{km}^2)$). To put the derived emission limits into context, see the box-percentile plots following (Figure 11), which demonstrate the distribution of emission limits in comparison with the distribution of Year 2012 existing emission rates at grid level in the SJV. Existing emission rates were distributed over a wide range between 0.01 up to $10,000 \text{ g}/(\text{h}\cdot\text{km}^2)$, with medians found close to $100 \text{ g}/(\text{h}\cdot\text{km}^2)$, higher than the medians of the emission limits.

Figure 11: Distribution of Derived Emission Limits Compared with Existing Emission Rates at Grid Level in the San Joaquin Valley



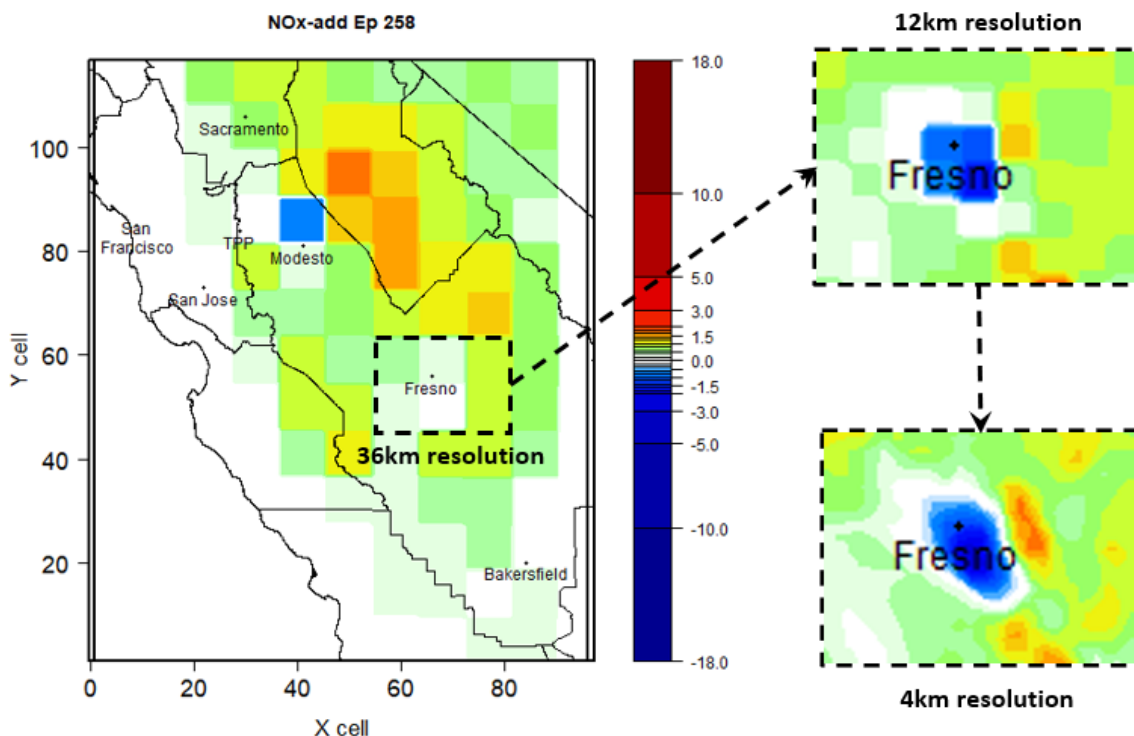
High-Resolution Benefits

Previous sections discussed the spatial heterogeneity in impact potential (S^+) and demonstrated its implications and applications for new source-siting screening, location-specific pollution control strategy design, and emission-limit derivation.

Compared with other tools of this kind, one salient advantage of the project's tool is its high resolution. High resolution involves not only high spatial resolution (4×4 km), but also high temporal resolution (hourly). With these high resolutions, the CMAQ_adj modeling tool used in this project can provide highly resolved, accurate information on how emission changes, at any given location, time, or precursor species, affect ozone in the SJV.

The Fresno and Southern SJV are the two important regions requiring high resolutions (4 km or higher) for both receptors across different meteorological conditions. Fresno is the only area that shows NO_x disbenefits for DAC O_x burdens in all three meteorology regimes, indicating a persistent VOC-limited ozone regime around its urban center. Its spatial reach, however, varies by episode. NO_x impact potentials (S^+) on the two sides of the regime's transition boundary can have opposite signs, which may not appear in low-resolution simulations (see Figure 12 as an example). Such smoothing out of the sharp spatial gradient in NO_x S^+ can be avoided through use of high-spatial resolution.

Figure 12: Example of how Coarse Grids Failed to Capture the Spatial Heterogeneity in Impact Potentials (S+)



The high temporal resolution at hourly level allows us to further investigate the temporal patterns of existing source contributions. Temporal patterns were informative in terms of answering questions such as: What are the effects of emission timing? Are same-day emission control actions effective for alleviating ozone levels on peak ozone days? How long does it take for upwind emissions to transport before they contribute to SJV's ozone formation? To well predict the air quality inside SJV "today", how many days in advance do we need to collect emission data from local and upwind sources? Are there any ozone chemistry regime changes throughout the day?

By spatially integrating existing source contributions in a time-resolved manner, the temporal patterns of source contribution by source regions can be quantified (Figure 13, Figure 14). The plots are presented in a backward time order, so the gray-shaded areas indicate the receptor time window (i.e., 8hr peak ozone hours "today"). Each bar represents the impacts of actual emissions at this specific hour from different source regions on receptors. Its unit is the same as the corresponding impact metric, so for our case, the unit is ppb. Subregions include San SFBSV, North/Middle/South SJV (NSJV/MSJV/SSJV) and other areas (North and South Central Coast, Mountain Counties).

Figure 13: Temporal Patterns of Existing Nox Contributions by Subregion

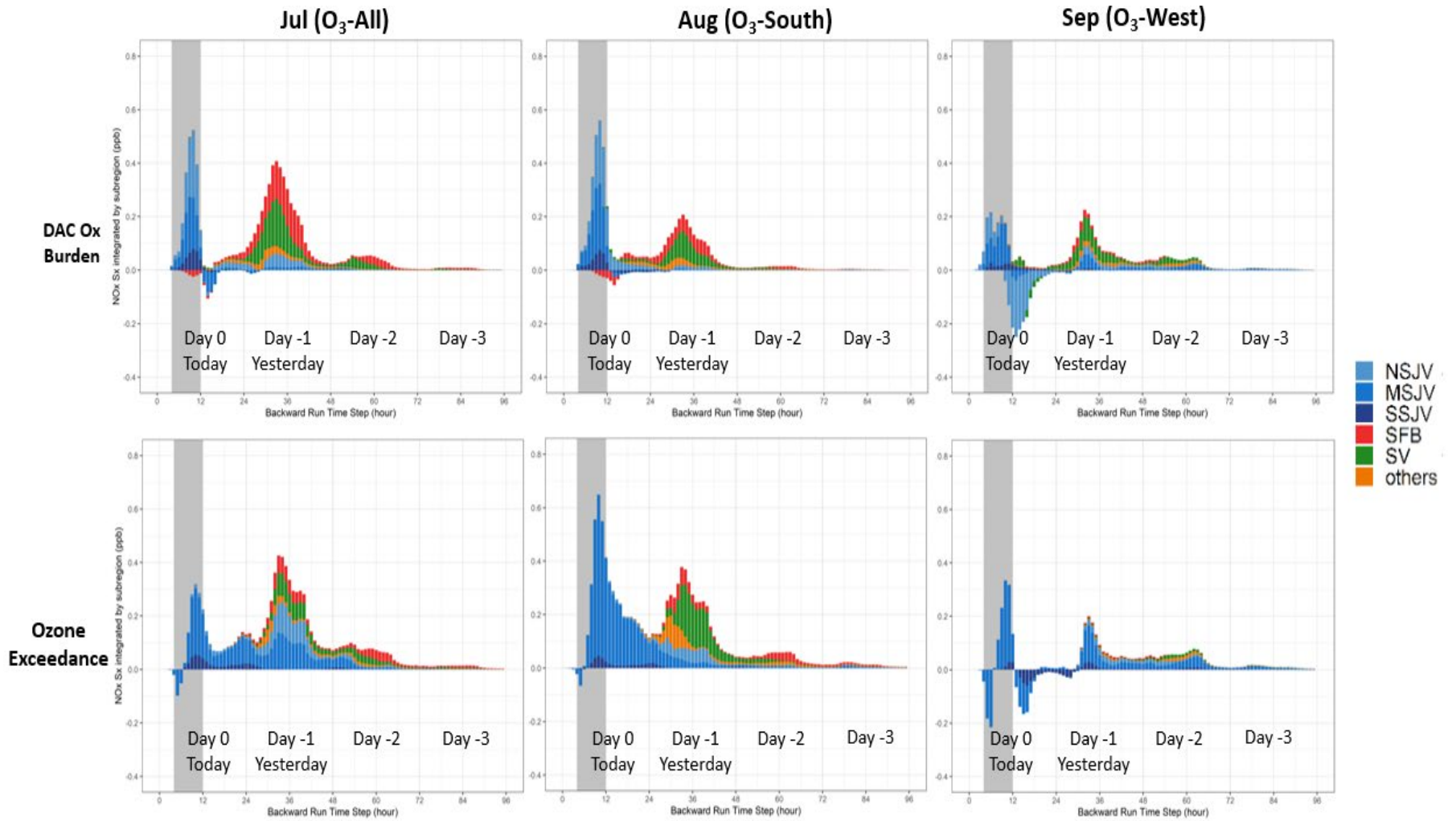
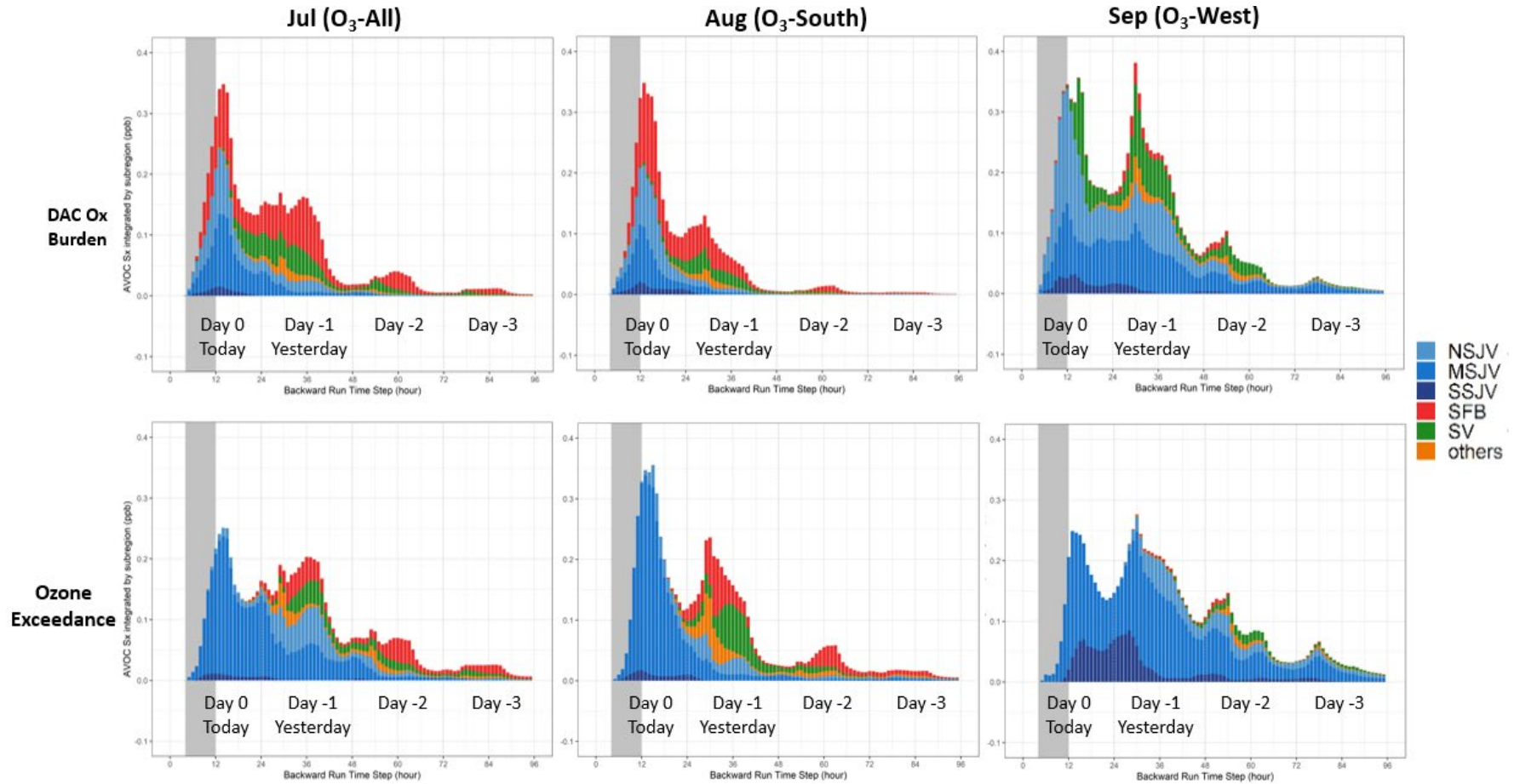


Figure 14: Temporal Patterns of Existing AVOC Contributions by Subregion



Analysis results reveal the contributions of precursors emitted in previous hours to the receptors "today." SV emissions tend to take around one day before contributing to receptors, as its same-day emission contributions are small across episodes. The temporal extent of influential SFB emissions depends more on meteorology and impact metrics.

For the DAC O_x burden receptor, NO_x contributions are mainly from same-day SJV emissions and upwind (SFB, SV) emissions on the previous day. In the AVOC case, SJV emission "today", SV emissions "yesterday", and SFB emissions on both days can all significantly contribute to DAC O_x burdens in July and August episodes. In the September episode, which has the largest local influence, SJV AVOC emissions during the last 3 days ("Day -2" to "Today") are all considerable contributors to the DAC O_x burdens on the last day. The SFB contribution in this episode will be very small due to the weakened onshore flows.

For the ozone exceedance receptor, in both NO_x and AVOC cases, SJV is always the dominating contributor across meteorological regimes. With stronger down-valley flows, upwind (SFB, SV) emissions during the past two days ("Day -2" to "yesterday") can still have impacts on ozone exceedance "today". However, with more stagnant conditions, upwind influences become very small, or even negligible in the AVOC case. Local contributions are mostly from northern SJV (NSJV) sources, and the influential time range also depends on flow characteristics. Generally, the ventilation in SJV is the most enhanced in the August (O₃-South) episode, followed by the July (O₃-All) episode, and the September (O₃-West) episode. Following this order, the influential SJV emissions in these episodes are from last 1, 2, and 4 days (including "today"), respectively.

Chapter Summary

This chapter delineated the primary outputs from our production runs – the impact potential maps of existing and potential source locations - and discusses its spatial heterogeneity under three different meteorological regimes.

Results shown that, in most locations, NO_x control is more efficient than AVOC control, either for reducing health burdens on disadvantaged communities or achieving policy compliance. VOC-limited (NO_x disbenefits) areas were commonly located around urban centers and the main north-south route but can also extend further to rural areas under stagnant conditions, implying stagnancy in SJV tends to shift ozone chemistry more towards VOC-limited.

Multiple applications of the impact potential maps were demonstrated, including but not limited to: new source siting optimization, location-specific emission control strategy design, emission limit derivation, and source attribution of existing emissions.

The high spatial (4km) and temporal (hourly) resolutions, advanced physical scheme and state-of-art chemical mechanism allow the adjoint tool to provide accurate and highly resolved outputs to support fine-scale emission control actions. In the meantime, the outputs can be easily coupled with emission scenario data for efficient impact evaluation. The calculation time needed is in the order of minutes. Chapter 4 will further illustrate these benefits of the tool through a detailed application case.

CHAPTER 4:

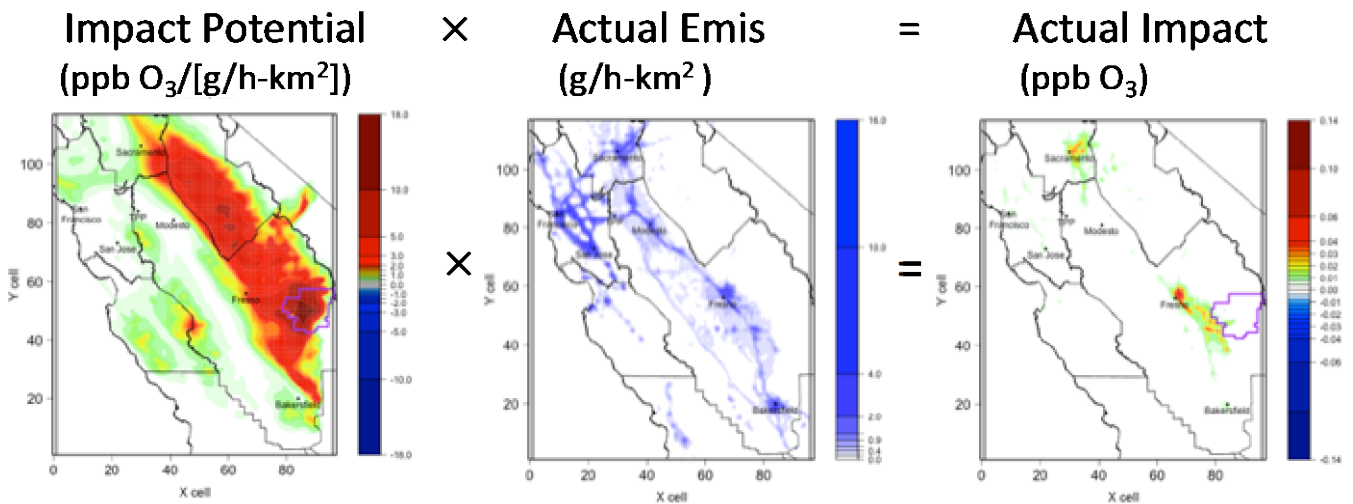
Case Study: Ozone Impact Evaluation for BDG Deployment Scenarios

Introduction

The impact potential (S^+) maps (Figure 6, Figure 7) developed in this project are effective tools for impact evaluation of numerous emission scenarios driven by different air quality policies. The procedure involves simple multiplication operations without any additional simulation work so that the impact evaluation is both accurate and efficient.

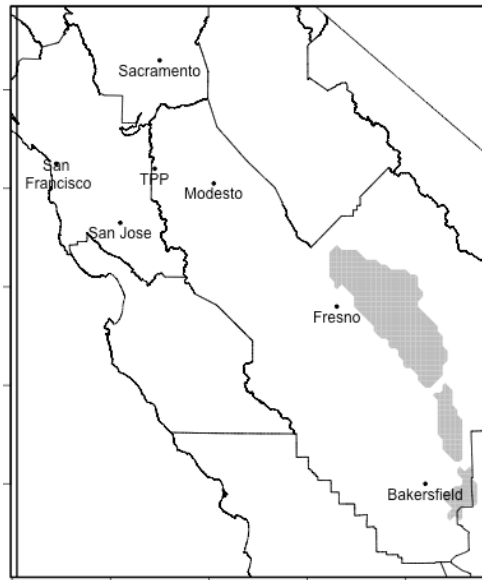
By multiplying the impact potential map with gridded emission data under each scenario, researchers can directly obtain the actual impact (as illustrated in Figure 15). Then the team spatially and temporally integrated the actual impacts for each scenario, which represent the receptor-wide impacts of emissions. Impact comparison between scenarios can then be easily conducted.

Figure 15: Illustration of the Impact Potential and Gridded Emissions Attributable to Source Locations



This chapter presents an illustrative application case. The project focused on the ozone exceedance receptor (defined in Chapter 2) and the July (O_3 -all) episode, which is a typical ozone-inducing meteorological regime with high temperatures and flow patterns that resemble the summer mean. In the application case, the team estimated the ozone exceedance impacts of the 32 BDG deployment scenarios driven by various policy decisions. The ozone exceedance area where peak 8-hour ozone concentrations exceeded 70 ppb under this meteorology is shown in gray in Figure 16.

Figure 16: Ozone Exceedance Area in July Episode, Shown in Gray



Background

Because California is actively diverting organic waste from landfills, a new organic waste recycling infrastructure is anticipated in the near future. How this system will be built is driven by the economics of organics handling facilities, as influenced by both market forces and policy incentives. A comprehensive analysis was conducted in 2020 to explore this economy using empirical data collected in California. On this basis, an Organic Recycling Facility Investment (ORFI) model was developed (Smith, 2020). This ORFI model mimics the private sector's profit-maximizing behaviors and predicts how California's biomass distributed generation (BDG) system will be developed under various scenarios.

In this chapter the team focused on 32 scenarios, each of which yields a BDG system through ORFI simulations. The 32 scenarios are the combinations of 4 electricity price levels, 4 bio-methane price levels, and 2 municipal solid waste (MSW) commingling scenarios:

Four Electricity Price Levels: Wholesale (e0), low (e1), medium (e2), high (e3)

Four Biomethane Price Levels: Wholesale (b0), low (b1), medium (b2), high (b3)

Two MSW Commingling Types: Complete separation of wet- and dry-waste streams (separate MSW), all MSW food/green/cardboard/paper wastes are commingled (commingled MSW)

Each BDG system from ORFI simulations consists of a suite of facilities expected to be built, including information about their locations, facility types, capacities, and feedstock intakes. Four facility types were considered in the model: dry anaerobic digestion (AD), wet AD, co-AD at wastewater treatment facilities (WWTF), and gasification. Two energy-product pathways were considered: electricity generation in combined heat and power (CHP) systems, and production of biomethane. In this model, all gasification facilities generate electricity, while AD facilities can choose between electricity and biomethane as the energy end-product.

With ORFI-simulated information, researchers could calculate the net emissions (relative to a no-BDG baseline system) of ozone precursors (NO_x, VOC) from each BDG system. Not only will the magnitude of net emissions vary by scenario, but also the locations of these net emissions will vary. By multiplying net emission maps with polluting potential (S^+) maps and spatially integrating the obtained multiplicative sensitivity (S^x) maps, the team can estimate net ozone impacts of these systems. The results capture both the impacts of different emission magnitudes and the impacts of facility-siting differences.

This approach required simple multiplication operations, so its computation costs are comparable to reduced-complexity models; but it is much more robust because it directly incorporates advanced physics and chemical mechanisms with high-resolution speciation. Such a quantitative understanding of ozone impacts from different systems can help regulatory agencies optimize both existing and future policies.

Methodology

In short, the procedure includes three main steps:

- Prepare net emission maps under each of the 32 BDG deployment scenarios.
- Multiply net-emission maps with impact potential (S^+) to get actual impact from individual source locations (i.e. S^x).
- Sum impact from individual source locations that will yield a scalar value representing the project impact from a given BDG deployment scenario.

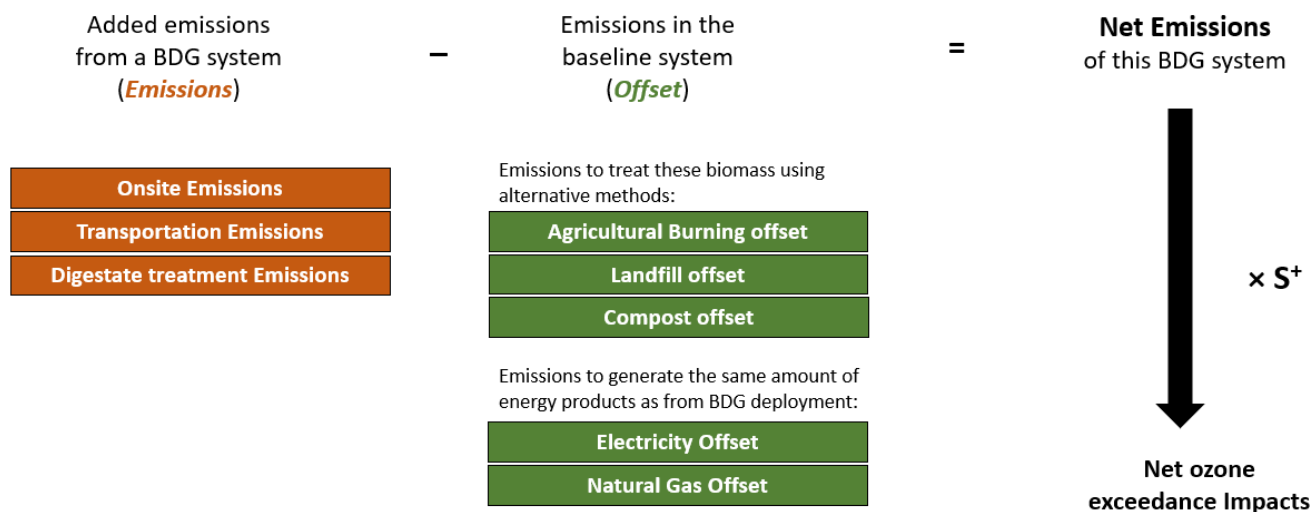
In this application case, the impact metric of ozone exceedance is defined as the peak 8-hour ozone concentrations in the exceedance area (Figure 22). For example, if the final impact value of a BDG system is 0.1 ppb, the average peak 8-hour ozone concentrations in exceedance areas are predicted to increase by 0.1 ppb when such a BDG system replaces the no-BDG baseline system.

For calculating net emissions of NO_x and VOC from a BDG system, researchers considered both the added emissions from the BDG system (emissions) and the emission offsets it brings (offsets). The latter equals the emissions in a no-BDG baseline system for processing the same amount of organic waste that is diverted to the BDG system.

The baseline system is assumed to be a hypothetical system that meets California's 75-percent reduction goal (diverting 75 percent of solid waste from landfills by 2025) without BDG deployment. In the baseline system, 18 subcategories of agricultural residues are identified as burnable (Scarborough et al., 2002) and burned on site. For all other organic wastes (except the 18 burnable subcategories), it is assumed that 75 percent goes to composting and 25 percent is sent to landfill in the baseline system.

Figure 17 summarizes the emission and offset layers considered for net-emission calculations. Eight layers were considered in this calculation procedure, including three emission layers and five offset layers.

Figure 17: Net Emission Calculation Procedure

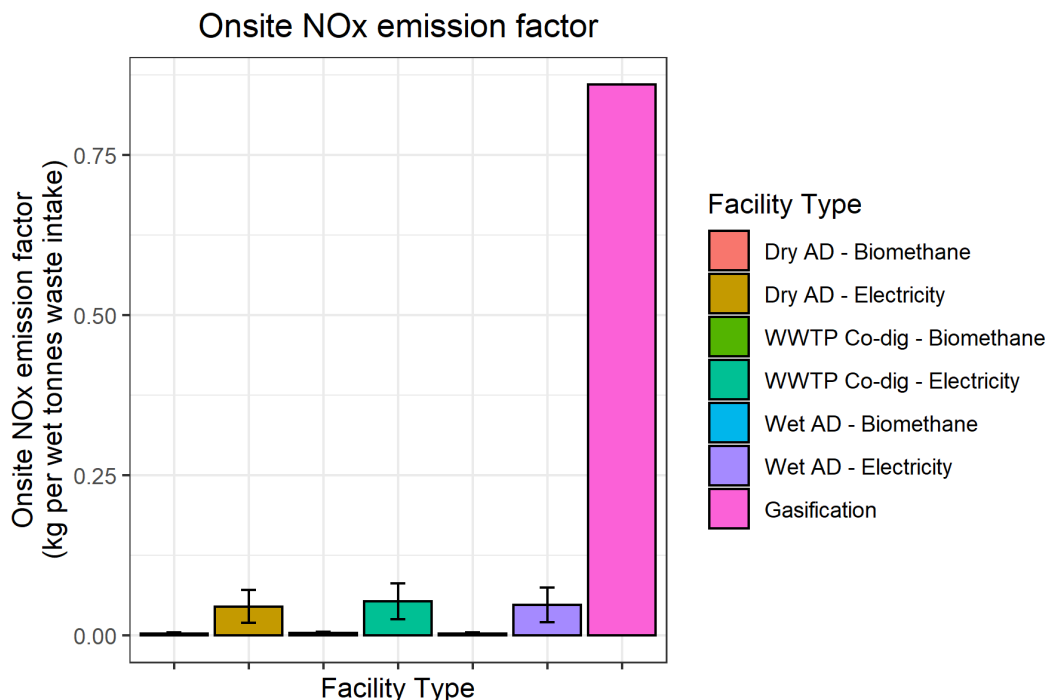


Annual totals of each emission/offset layer are first calculated by multiplying waste intake at BDG facilities with corresponding emission factors. Unless stated otherwise, most of the emission factors used in this analysis are derived from a recent paper that listed emission factors involved in organic-waste management lifecycles (Nordahl et al., 2020). The original emission factors are assembled from multiple sources, including peer-reviewed articles, the Greenhouse gases, Regulated Emissions, and Energy use in Technologies Model (GREET), the Ecoinvent database, and the authors’ measurement data. These emission factors are converted to the unit of kg pollutants emitted per wet tons of waste intake, and are then multiplied with the waste intake to calculate annual emissions of NO_x and VOC. These annual values are then spatially and temporally distributed to obtain an hourly-resolved emission map in the SARMAP domain.

Calculation details of each *emission-category layer* follow.

Onsite Emissions: This layer represents pollutants directly emitted at BDG facilities. Recall that four facility types (dry AD, wet AD, co-AD at WWTF, and gasification) and two energy-product pathways (electricity generation in CHP systems and production of biomethane) were considered in the project model. For facilities with electricity as their energy product, emission rates measured in a previous study at a dry AD facility in California are assumed for electricity generation from biogas combustion and biogas flare (Scown et al., 2019). These emissions are assumed to be representative for the same processes at dry AD, wet AD, and wastewater treatment plant (WWTP) co-digestion AD facilities. Onsite emissions at gasification facilities are derived from a 2013 study (Zaman, 2013). For facilities with biomethane as their energy product, emissions from biogas upgrading and flaring are considered, with emission factors sourced from Nordahl et al. (2020). Significant discrepancies exist among facility types in terms of the onsite NO_x emission factor (Figure 18). It is noteworthy that gasification facilities tend to have a much higher onsite NO_x emission factor than all other AD facilities. Onsite emissions are spatially distributed to corresponding facilities and assumed to be continuous in time.

Figure 18: Onsite NO_x Emission Factor of Each Facility Type



Transportation Emissions: This layer represents the emissions for transporting biomass wastes from their generation sources to BDG facilities. Since the source locations of waste intakes are also provided in the ORFI model, the transportation distance can be easily determined. Flatbed trucks are assumed to be the main vehicle for both pickup and delivery of waste biomass, and emission factors are derived from an emission factor (EMFAC) 2007 model (California Air Resources Board, 2007). For each BDG facility, transportation emissions are spatially distributed to a buffer zone around the facility, with the radius approximated as the intake-weighted average transportation distance. Transportation emissions are assumed to happen every weekday between 6 a.m. and 4 p.m. The emission schedule is based on biomass-transport drivers’ job descriptions and drivers’ discussions online (Indeed, 2021).

Digestate Compost Emissions: This model assumes an outdoor composting operation for digestate treatment, so this layer represents the emissions from digestate composting. Emission factors are sourced from Nordahl et al., (2020). Emissions from organic waste composting and digestate composting are different in magnitude because digestates are more biologically stable if feedstocks are processed at AD facilities for an adequate period of time. Digestate compost emissions are spatially distributed to the closest composting sites around a BDG facility and considered continuous in time.

Agricultural Burning Offset: This layer represents the agricultural burning emissions that will result if organic waste in a specific system is not diverted to BDG. Only 18 subcategories of agricultural residues are burnable and contribute to agricultural burning offsets. Emission factors are sourced from a California Air Resources Board’s report (2002). Although the team includes agricultural burning offset in net emission calculation, it is excluded from net ozone impacts calculation. The San Joaquin Valley Air Pollution Control District (SJVAPCD) has its

burn permit program, which will constrain open burning around high-ozone days. The team therefore assumed negligible ozone impacts from agricultural burning offsets on ozone exceedance. This assumption could result in an underestimation of BDG air-quality benefits.

Landfill Offset: This layer represents emissions from landfills that will otherwise occur if the organic waste in a specific system is not diverted to BDG. In a baseline system without BDG development, 25 percent of organic waste will be landfilled. This offset is spatially distributed to the closest landfill sites around a BDG facility and considered continuous in time.

Compost Offset: This layer represents the emissions from composting that will otherwise happen if the organic waste in a specific system is not diverted to BDG. In a baseline system without BDG development, 75 percent of the organic waste will be sent to composting facilities. This offset is spatially distributed to the closest composting sites around a BDG facility and considered continuous in time.

Electricity Offset: This layer represents the emissions that will otherwise happen in the baseline system for generating the same amount of electricity as generated in a BDG system. The net amount of electricity generation in a BDG system is applied here since electricity consumption in this BDG system is already subtracted from its electricity generation. Emission factors are sourced from Nordahl et al., (2020). This electricity offset is spatially distributed to California's natural gas combined cycle (NGCC) power plants (proportional to their capacities) and is continuous throughout the year.

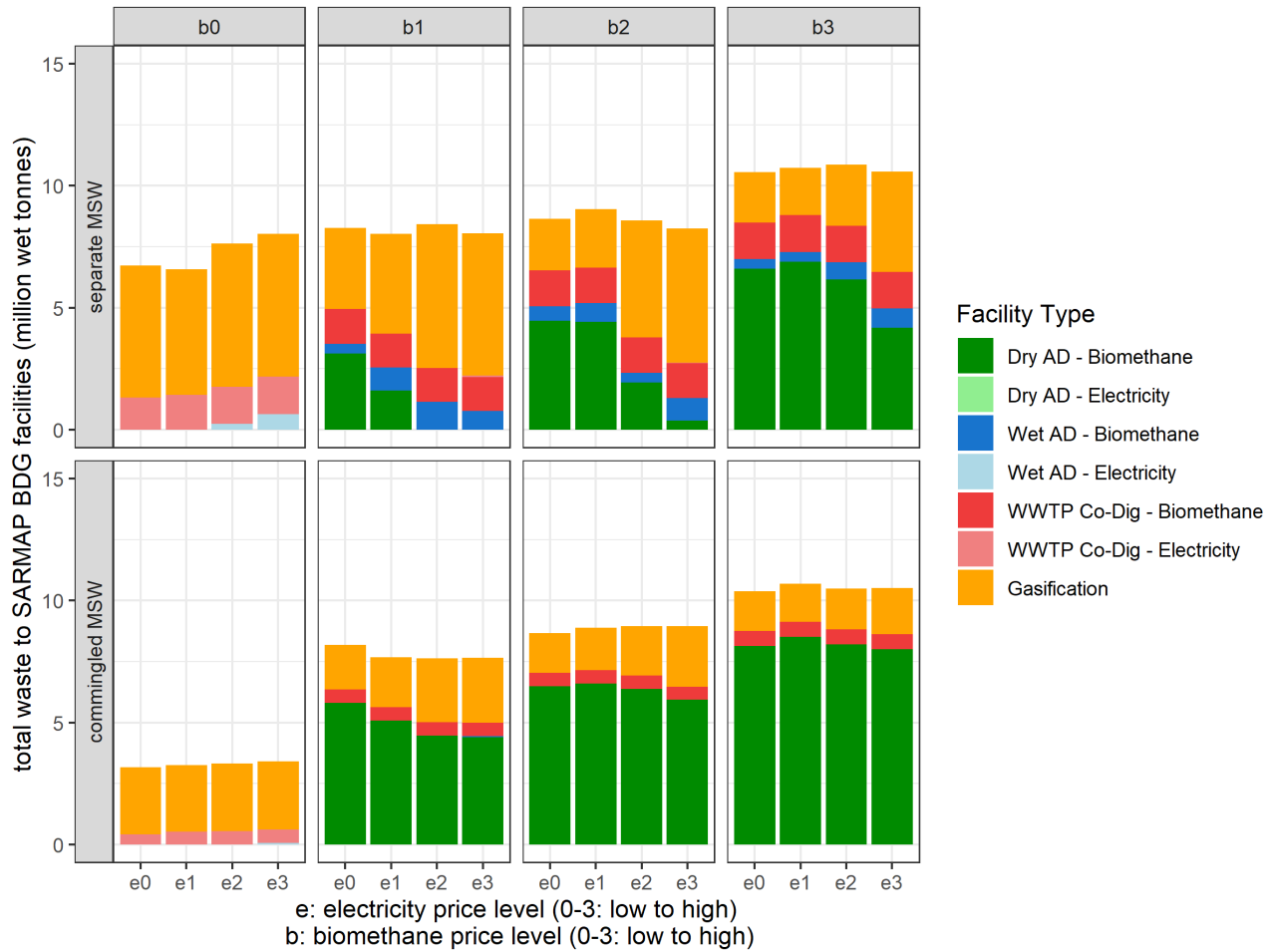
Natural Gas Offset: This layer represents emissions that will otherwise happen in the baseline system for generating the same amount of biomethane as generated in a BDG system. Emissions from both extraction and processing stages were considered, with contributions of each quantified using the GREET 2020 model (Argonne National Laboratory, 2020). The biomethane offset is spatially distributed to natural gas production wells and processing plants based on their relative contributions in GREET 2020. This emission layer is also assumed to be continuous over time.

BDG Deployment Systems

In the 32 BDG systems included in this application case, about 7.1 to 24.1 million tons of organic waste are diverted to biomass distributed generation (BDG) facilities in California; about 40 percent to 50 percent are sent to facilities within the SARMAP domain. This percentage does not change significantly across scenarios. As this application case focuses on SARMAP domain and ozone exceedance inside the SJV, all results shown here are for the SARMAP domain.

Figure 19 presents the total waste sent to SARMAP facilities in each system, ranging from 3.2 million tonnes (under the lowest wholesale biomethane price b0, with commingled MSW) to 10.9 million tonnes (under the "high" biomethane price b3, with separate MSW).

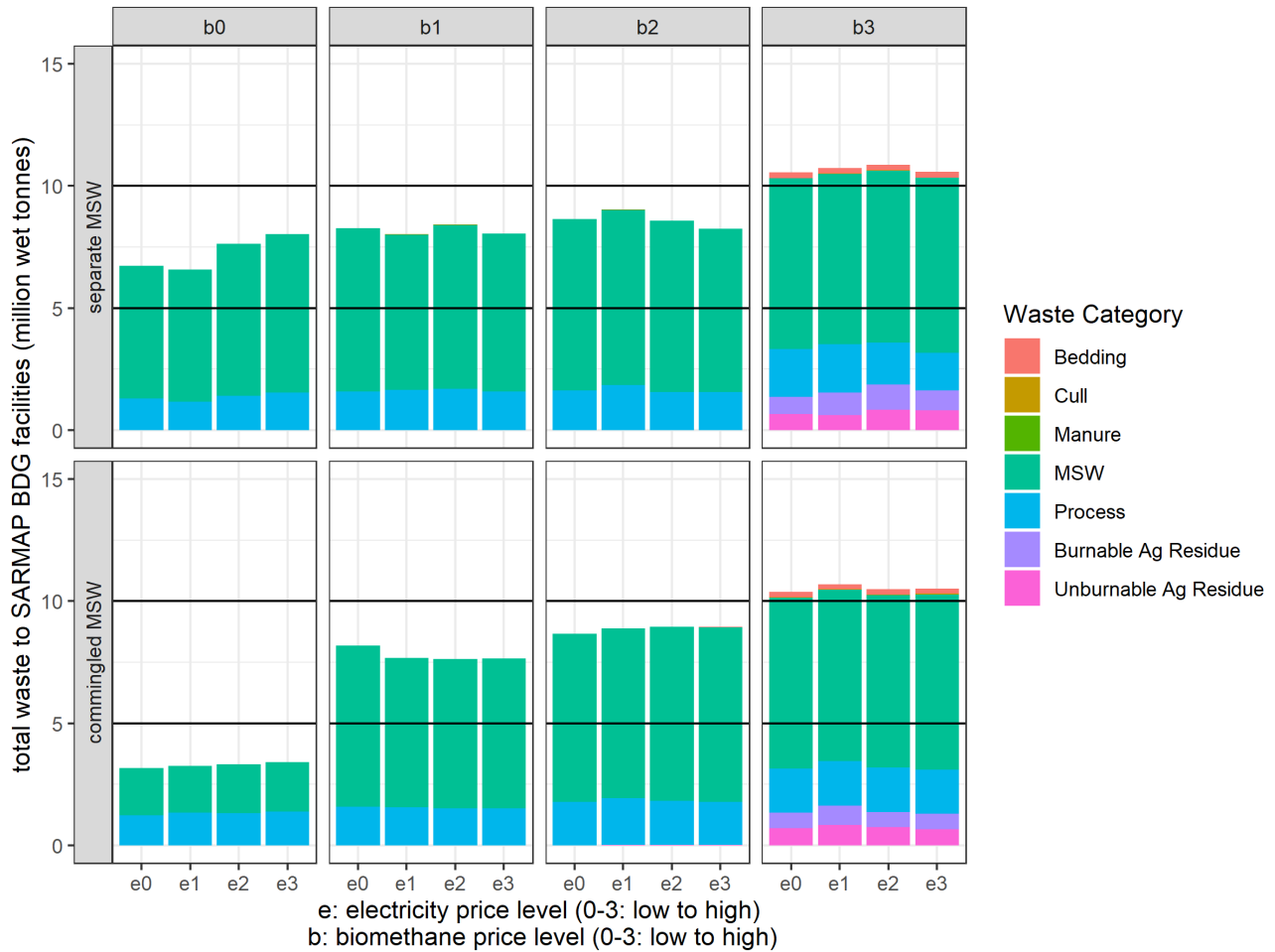
Figure 19: Total Waste Sent to Each Facility in the SARMAP Domain



Biomethane prices are the main drivers of changes in waste-intake totals. At the lowest wholesale biomethane price level (b0), new facilities generate electricity when it is most financially beneficial. When biomethane prices rise, more organic waste will be diverted from landfills to BDG facilities that generate biomethane. High waste intake occurs at the highest biomethane price, regardless of the other two conditions.

Electricity prices, on the other hand, do not significantly shift waste-intake totals, but do influence the relative importance of gasification and dry AD facilities. Higher electricity prices encourage more waste to be sent to gasification for generating electricity, and less waste to dry AD facilities. Because gasification is associated with a much higher onsite NO_x emission factor than a dry AD, systems under different electricity prices will have different onsite NO_x emissions (Figure 20), even though waste-intake totals may be similar.

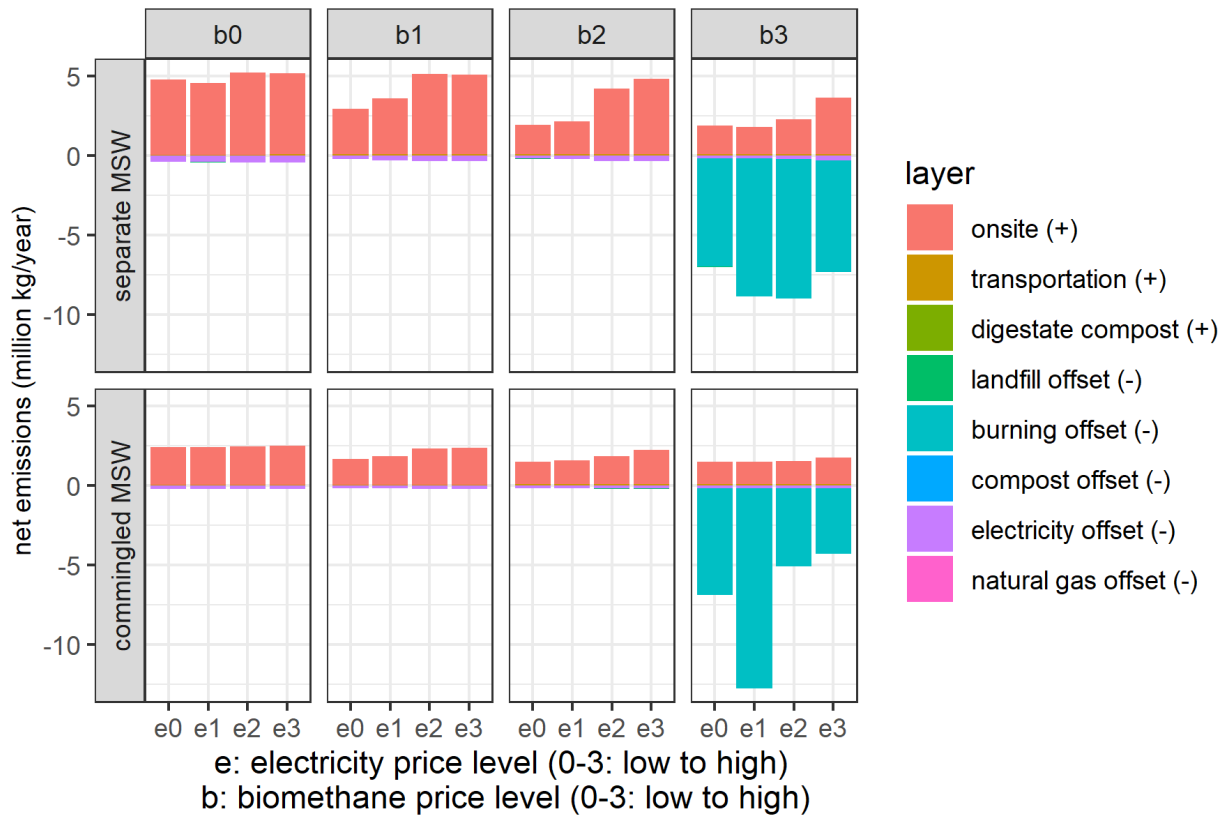
Figure 20: Total Waste in Each Category Sent to SARMAP Facilities



When comparing separate and commingled MSW scenarios, their differences mostly concern facility type. The commingled MSW waste stream is not suitable for processing at wet AD, WWTP co-digestion, or gasification. This explains commingled MSW scenarios' heavy reliance on dry AD facilities. In terms of total waste intake, the differences between separate and commingled MSW are only obvious at the lowest wholesale biomethane price (b0). At this price, no biomethane facilities will be built, and commingled MSW will further limit the low-moisture waste that can be sent to gasification facilities. Therefore, the smallest waste intake is found with b0 and commingled MSW.

Figure 21 shows the breakdown of waste intake by feedstock category, which mainly consists of MSW and food-processing waste. In high-waste intake cases, when biomethane prices are high, agricultural residue is diverted to bioenergy facilities. Agricultural burning offsets, which emit significant NO_x , will only occur in these high-waste intake cases.

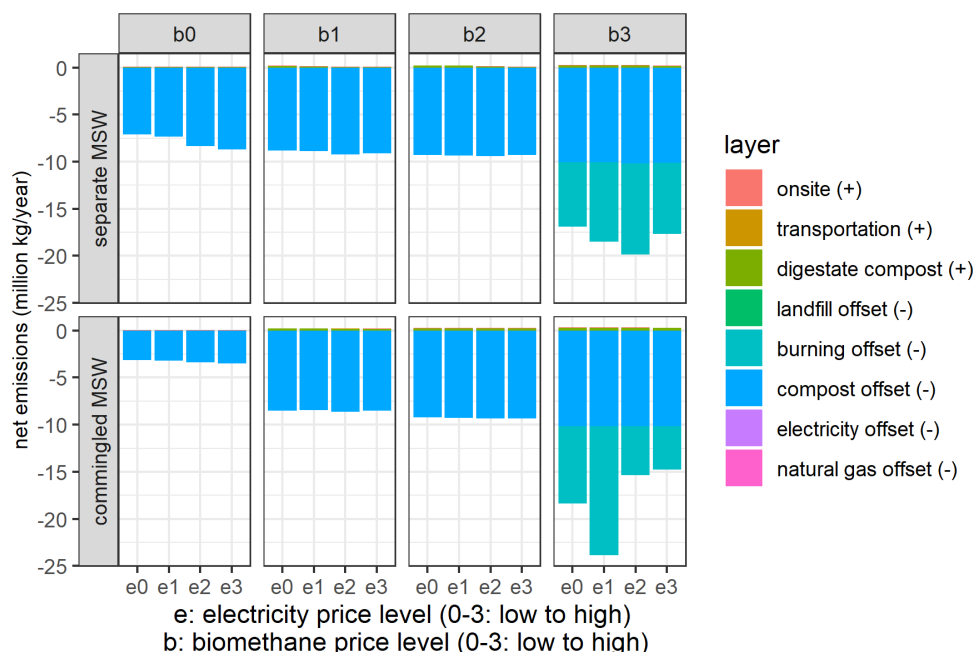
Figure 21: Net NO_x Emissions, by Scenario



Net-Precursor Emissions

Following the calculation procedure shown in Figure 20, net emissions of NO_x and VOC from each of the 32 BDG systems were calculated. Figure 22 shows net NO_x emissions of each source category, as colored by its emission/offset layer. Compared with onsite emissions, emissions from transportation and digestate composting are negligible. In cases when biomethane prices are high (b3), burnable agricultural residue is diverted to processing facilities, creating a burning offset. Thus, only high-waste intake systems have negative net NO_x emissions. For others, net NO_x emissions are positive. Considering the assumption that negligible ozone exceedance impacts from agricultural burning offsets are due to burn permit restrictions, onsite NO_x emissions are the main driver of NO_x-related ozone exceedance impacts. Since the siting of new BDG facilities varies greatly by scenario, projections of onsite NO_x emission locations will also be variable. This underscores the importance of capturing siting impacts, which are shown in the project’s polluting-potential maps.

Figure 22: Net VOC Emissions by Scenarios



The magnitude of net NO_x emissions is largely influenced by the percentage of gasification facilities. High temperatures at gasification facilities will cause significant thermal NO_x emissions in the process. As already shown in Figure 18, the onsite NO_x emission factor at gasification facilities is much larger than that at dry AD facilities. Because higher electricity prices will create more waste for gasification facilities and less for dry AD (especially in the separate MSW scenario), an increase in emissions will mean higher electricity prices, although the total waste intake in these cases remains similar. As for biomethane price, its effect is the opposite. Higher biomethane prices send more waste to dry AD and less to gasification. Although a higher biomethane price also increases total waste intake, there is a decrease in net NO_x emissions as biomethane prices transition from wholesale (b0) to high (b3).

Figure 23 shows a consistently negative net VOC emission across scenarios. In other words, VOC offsets are always much larger than added emissions in any BDG emission category. Still, burning offsets only occur in high-waste intake cases when biomethane prices are high. In other cases, compost offsets dominate. Compared with onsite NO_x emissions, compost offsets are more proportional to the amounts of waste intake. Since composting offsets are always spatially distributed to existing composting facilities, the locations of this offset are also more stable across different scenarios.

In summary, the research team drew two key conclusions about net-precursor emissions. First, net NO_x is mostly positive (except in high-waste intake cases) and net VOC is always negative. An impact assessment that considers both precursors is therefore needed to interpret whether BDG deployment brings net air-quality benefits or extra-ozone burdens. Second, net NO_x is mainly driven by onsite NO_x emissions, which highlights the necessity of strategic siting decisions. The negative net VOC is mainly from significant compost VOC offsets.

Net Ozone Exceedance Impacts of 32 BDG Scenarios

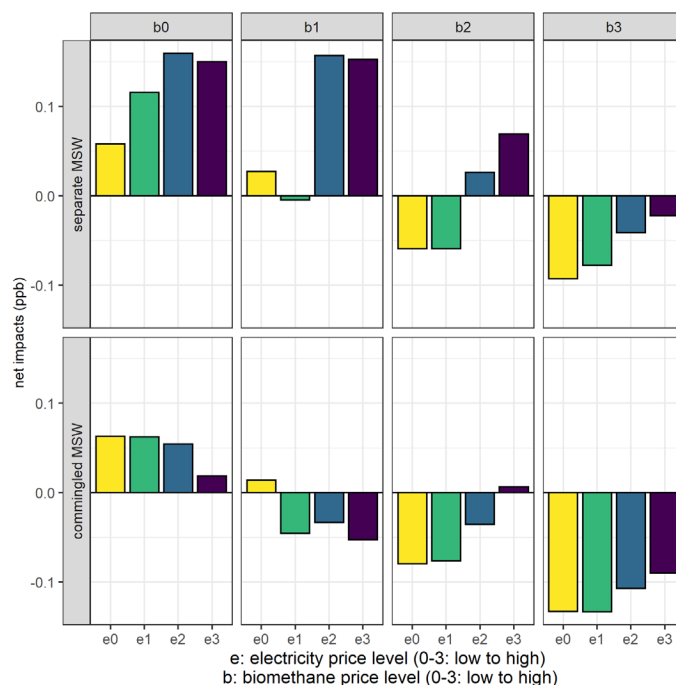
After calculating annual totals of net-precursor emissions, the team spatially and temporally distributed these values to prepare an hourly resolved net-emission map based on the assumptions described in the methodology section. These spatially and temporally resolved net emission maps were then multiplied with impact potential (S+) maps to obtain multiplicative-sensitivity maps. The S^x maps were then spatially and temporally added to estimate the net ozone exceedance impacts of the specific scenario.

The final result is a scalar value for each BDG scenario that represents net changes in 8-hour peak-ozone concentrations in SJV exceedance areas, assuming a switch from the baseline system to the corresponding BDG system. A positive value indicates there are extra ozone burdens from BDG development, while a negative value implies that BDG development brings net air-quality benefits.

Project analysis focuses on the July (O_3 -all) episode since its flow patterns resemble summer average patterns, while the episode-average temperature is above summer averages. The down-valley flows push pollutants to the southern end of the valley, near the foot of mountains where exceedance areas are typically found. The net-ozone exceedance impacts of 32 scenarios in this episode can be compared against one another.

Figure 23 presents the net ozone exceedance impacts of the 32 scenarios, in the range of -0.13 to 0.16 ppb. Considering that this value represents an ozone concentration change averaged over the 8,192 km² ozone-exceedance area (shaded, in Figure 16), it is not a negligible magnitude so is worth consideration. The optimal BDG system is found at the highest biomethane price with low (or wholesale) electricity price and commingled MSW. The worst case is at the lowest biomethane price with highest electricity price and separate MSW.

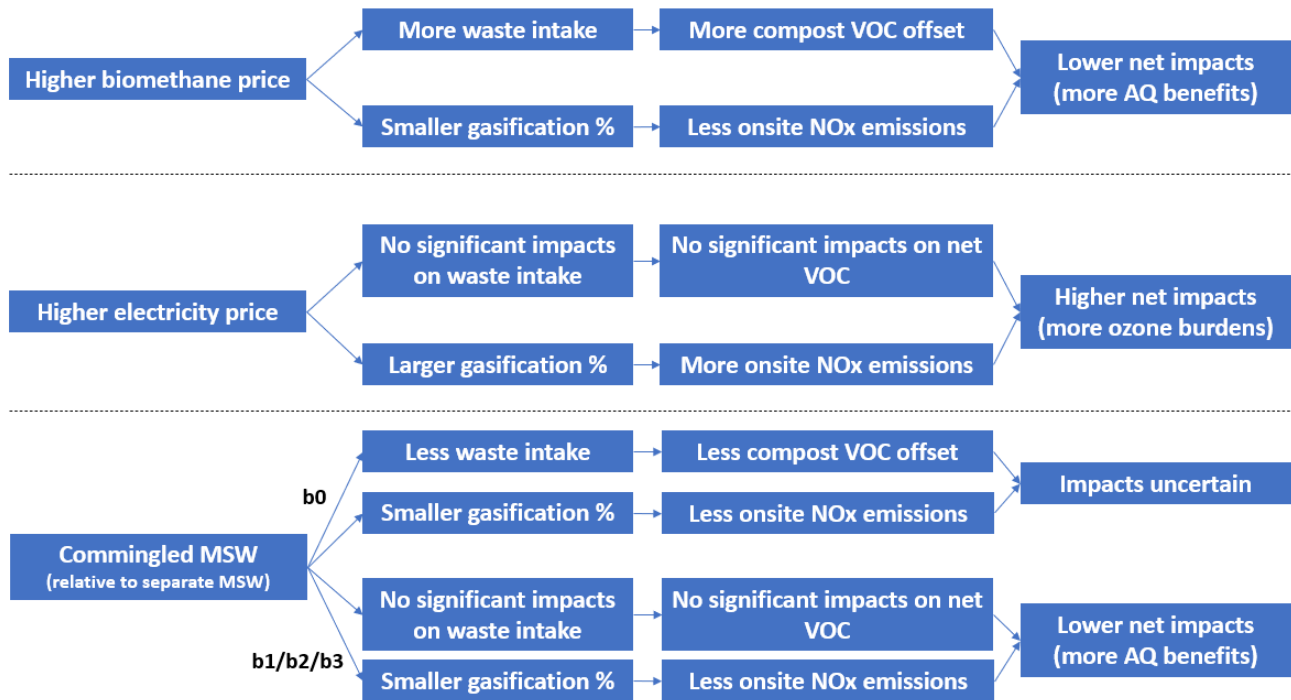
Figure 23: Net Ozone Exceedance Impacts Under 32 BDG-Development Scenarios



The differences in net impacts between scenarios can be primarily interpreted as two parts: the impacts of differences in net precursor emissions, which are driven directly by energy prices and MSW commingling assumptions; and the location (siting) impacts of emission sources, especially for onsite NO_x emissions.

For the first part, generalized relationships can explain how assumptions on energy prices and the MSW commingling type influence waste intake and facility type, thus changing net precursor emissions and ultimately resulting in different net impacts. Each of these relationships is discussed here and summarized in Figure 24.

Figure 24: Generalized Relationships Between Assumptions and Net Impacts, without Consideration of Siting Impacts



Biomethane Price: A higher biomethane price will enhance BDG waste diversion and lead to a larger compost VOC offset. At the same time, more waste will be incentivized to be sent to biomethane-generating dry AD facilities instead of electricity-generating gasification facilities, which will result in lower onsite NO_x emissions. Both changes will be beneficial for local air quality.

Electricity Price: Electricity price does not significantly influence total waste intake, so offset magnitude is quite stable under different electricity prices. However, a higher electricity price will make gasification facilities more economically feasible. With more waste diverted from AD to gasification, onsite NO_x emissions will rise, theoretically bringing extra pollution burdens to the area.

MSW Commingling: When biomethane price is not at its lowest level (b0), MSW commingling does not impact total waste intake. However, because the mixed-waste stream can only be processed at dry AD facilities, gasification capacity will be reduced in commingled

MSW cases. That said, when the biomethane price is low, medium, or high (b1/b2/b3), MSW commingling will decrease onsite NO_x emissions and lead to more air-quality benefits. Finally, in cases with wholesale biomethane prices (b0), outcomes are more complicated to predict because waste intake and VOC offset will both decrease when MSW is mixed.

There are some obvious differences between derived relationships (Figure 24) and actual patterns in net ozone-exceedance impacts (Figure 23). For example, in Figure 23 when electricity price is highest (e3), increasing the biomethane price (from b1 to b2) increases ozone burdens, which contradicts the theoretical relationship shown in Figure 27. Such inconsistencies can only be explained by location (siting) impacts.

Importance of Facility Siting

The gap between theoretical relationships (summarized in Figure 24) and actual patterns in ozone impacts (Figure 23) show the importance of facility siting. Due to the spatial heterogeneity in polluting potentials (S^+), the same amount of net emissions may result in different ozone impacts depending on where emission sources are located. While VOC compost offset occurs at existing composting facilities with stable locations across scenarios, the locations of onsite NO_x vary greatly by scenario, depending upon the locations of the facilities. As a result, onsite NO_x is the major driver of siting impacts.

Figure 25 shows the relationship between onsite NO_x emissions and their ozone exceedance impacts in the July episode. In general, lower onsite NO_x emissions are associated with smaller ozone exceedance impacts. However, decreased impacts are not always proportional to decreased emissions (for example, points between the orange arrow). Sometimes, decreased emissions can even lead to increased impacts (for example, points between the blue arrow).

Figure 25: Relationship Between Onsite NO_x Emissions and Their Ozone Exceedance Impacts

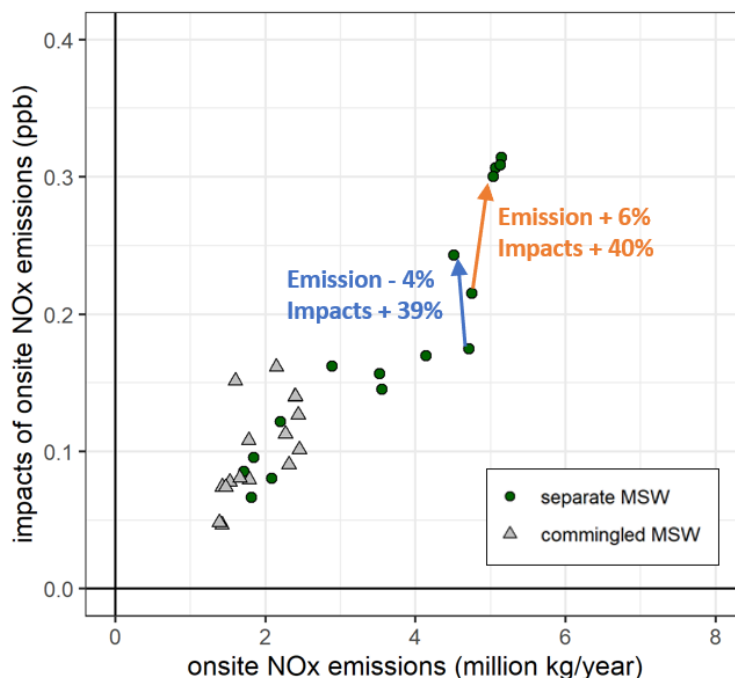
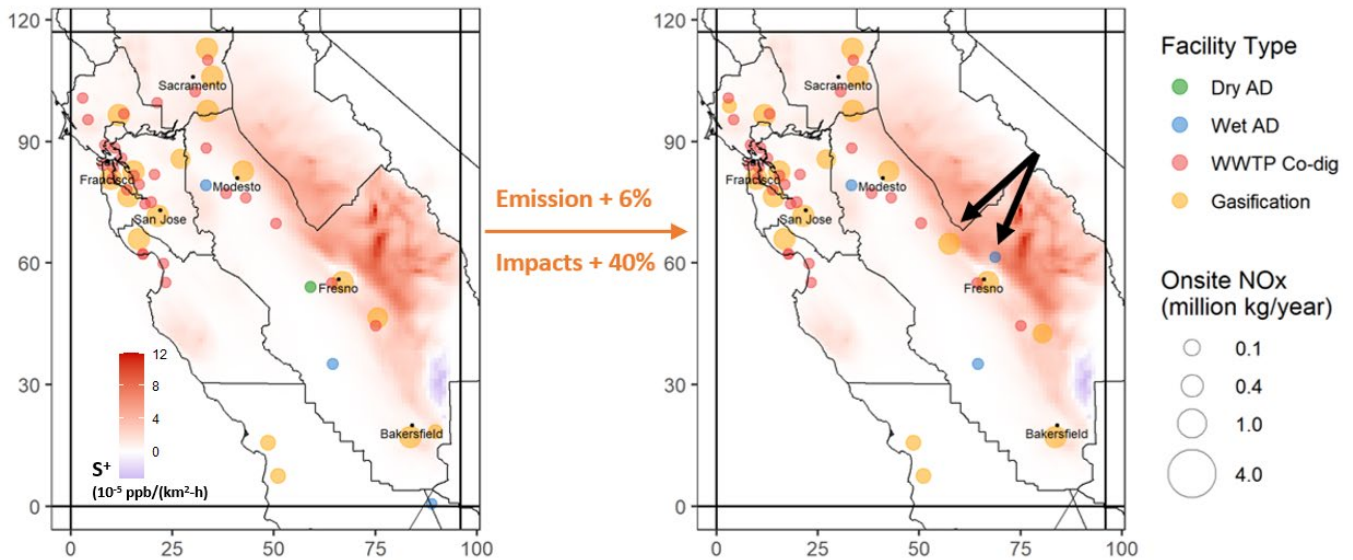


Figure 26 shows two siting scenarios. From left to right, there is only a 6-percent increase in onsite NO_x emissions, while its ozone exceedance impact increases by 40 percent. This dramatic increase in ozone impacts is rooted in the siting of BDG facilities in Figure 32 (impact potential is shown with a red background). It is obvious that two new facilities (pointed to by black arrows) are built in polluting potential hotspot areas and will thus significantly contribute to SJV's ozone exceedance. In future bioenergy development efforts, siting decisions like these should be strategically avoided. Otherwise, even if the emission magnitude is well controlled, its impacts on ozone burdens cannot be efficiently mitigated.

Figure 26: An Illustrative Example of Siting Importance



Chapter Summary

This chapter presented a detailed application case where impact-potential (S^+) maps generated in this project were used for the ozone exceedance impact evaluation of 32 BDG deployment scenarios. This evaluation approach was both accurate and efficient.

Organic waste management systems were examined under 32 bioenergy development scenarios. Net emissions from each emission category were calculated and multiplied with the impact potential map to estimate their net impacts on SJV's ozone exceedance. Depending on energy price and municipal solid waste (MSW) commingling type, net ozone impacts averaged in the range between -0.13 to 0.16 ppb. Net impacts are mainly driven by onsite NO_x emissions at processing facilities and compost VOC offsets at composting facilities. The dramatic importance of facility siting was demonstrated and discussed, which was made possible only by the use of the CMAQ_adj tool built by this project.

CHAPTER 5:

Conclusions

This project focused on the SJV to conduct this first-of-its-kind study to quantify the relative importance of individual source locations according to their ozone impacts (quantified by impact potential), on disadvantaged community ozone burdens and on non-attainment episodes. The SJV was chosen because it has abundant biomass waste streams and has long been out of compliance with NAAQS, leading to the area's top ranking among the state's disadvantaged communities. The geospatial datasets generated through this project filled the knowledge gap in location-specific emission controls and pollution-mitigation strategies that could be leveraged in the planning stages of distributed generation development. The project demonstrated the application of the resulting tool and datasets for mitigating regulatory challenges for future scale-up of BDG for this region.

Further application of the adjoint modeling tool used in this project is recommended to unlock its full potential. First, as the adjoint tool is receptor oriented, it is well suited to designed communities — or receptor-oriented strategies. While in this current project influential sources were mapped according to their impacts on ozone burden across all disadvantaged communities, in future work specific AB 617 communities can be selected as receptors of interest for identifying both their respective influential source locations and emission timing.

Secondly, as pollution impacts are determined by the adjoint tool for individual source locations and emission hours, they can also be applied to evaluating the environmental impacts of emission changes that may occur unevenly in space and time. For example, current electric vehicle adoption takes place primarily in the more affluent communities, which resulted in a non-uniform reduction in on-road emissions. In contrast, traditional forward sensitivity analyses, which generally assume proportional emission changes in a given sector, are not suitable.

Third, the adjoint tool can be used to achieve co-benefits. In this study, the impact metrics are defined for ozone. Alternatively, the impact metrics can be defined for multiple pollutants (for example, both ozone and PM_{2.5}) so that the impact potential of a given emission source can be determined accounting for its contribution to all the pollutants of interest. Location and time-specific emission control strategies can therefore be identified to maximize co-benefits.

To summarize, the analysis tool and framework developed through this project can be extended in future work to include other criteria pollutants and greenhouse gases, other major air basins in California, future emission years, and emission-change scenarios.

GLOSSARY AND LIST OF ACRONYMS

Term	Definition
AD	Anaerobic Digestion
AVOC	Anthropogenic volatile organic compound
AGU	American Geophysics Union
B0	Wholesale biomethane price level
B1	Low biomethane price level
B2	Medium biomethane price level
B3	High biomethane price level
BCON	Lateral Chemical Boundary Conditions
BDG	Biomass Distributed Generation
BF	Brute-force
BVOC	Biogenic volatile organic compound
CalEPA	California Environmental Protection Agency
CARB	California Air Resources Board
CHP	Combined Heat and Power
CPUC	California Public Utilities Commission
CTM	Chemical transport model
CMAQ	Community Multiscale Air Quality Model
CMAQ_adj	The adjoint of the CMAQ model that attributes ozone changes in a receptor region to all possible individual emission sources
DAC	Disadvantaged Communities
DDM	Direct decoupled method
E0	Wholesale electricity price level
E1	Low electricity price level
E2	Medium electricity price level
E3	High electricity price level
EMFAC	CARB Emission Factor model
GREET	The Greenhouse gases, Regulated Emissions, and Energy use in Technologies Model
ICON	Initial Chemical Conditions
MC	Mountain Counties
MM5	Mesoscale Meteorological Model Version 5
MOZART	Model for Ozone and Related chemical Tracers

Term	Definition
MSJV	Middle San Joaquin Valley
MSW	Municipal Solid Waste
NAAQS	National Ambient Air Quality Standards
NCC	North Central Coast
NGCC	Natural Gas Combined Cycle power plants
NSJV	North San Joaquin Valley
NO	Nitrogen monoxide
NO ₂	Nitrogen dioxide
NO _x	Nitrogen oxides
NOAA	National Oceanic and Atmospheric Administration
O _x	Odd oxygen, which is the sum of ozone and nitrogen dioxide
O ₃	Ozone
ORFI	Organic Recycling Facility Investment
PBL	Planetary Boundary Layer
ppm	Parts per million by volume
ppb	Parts per billion by volume
SAPRC	Statewide Air Pollution Research Center
SARMAP	SJVAQS/AUSPEX Regional Modeling Adaptation Project
SCC	South Central Coast
SFB	San Francisco Bay Area
SJV	San Joaquin Valley
SSJV	South San Joaquin Valley
SV	Sacramento Valley
TAC	Technical Advisory Committee
UTV	Coordinated Universal Time
VOC	Volatile organic compound
WWTP	Wastewater Treatment Plant

References

- Argonne National Laboratory. 2020. *Summary of E1xpansions and Updates in GREET 2020*.
- Bastien, L.A.J., B.C. McDonald, N.J. Brown, and R.A. Harley. 2015. "High-Resolution Mapping of Sources Contributing to Urban Air Pollution Using Adjoint Sensitivity Analysis: Benzene and Diesel Black Carbon". *Environ. Sci. Technol.* 49, 7276–7284. Available at <https://doi.org/10.1021/acs.est.5b00686>.
- Byun, D. and K.L. Schere. 2006. "Review of the Governing Equations, Computational Algorithms, and Other Components of the Models-3 Community Multiscale Air Quality (CMAQ) Modeling System". *Appl. Mech. Rev* 59, 51–77. Available at <https://doi.org/10.1115/1.2128636>.
- California Air Resources Board (CARB). 2007. *EMFAC2007 Version 2.30 User's Guide*.
- Carreras-Sospedra, M., R. Williams, and D. Dabdub. 2016. "Assessment of the emissions and air quality impacts of biomass and biogas use in California". *Journal of the Air & Waste Management Association* 66, 134–150. Available at <https://doi.org/10.1080/10962247.2015.1087892>.
- Carter, W.P.L. 2010a. "Development of the SAPRC-07 chemical mechanism". *Atmospheric Environment, Atmospheric Chemical Mechanisms: Selected Papers from the 2008 Conference* 44, 5324–5335. Available at <https://doi.org/10.1016/j.atmosenv.2010.01.026>.
- Carter, W.P.L. 2010b. "Development of the SAPRC-07 chemical mechanism". *Atmospheric Environment, Atmospheric Chemical Mechanisms: Selected Papers from the 2008 Conference* 44, 5324–5335. Available at <https://doi.org/10.1016/j.atmosenv.2010.01.026>.
- Carter, W.P.L. 2000. *Documentation of the Saprc-99 Chemical Mechanism for Voc Reactivity Assessment Volume 1 Of 2 Documentation Text 231*.
- Cohan, D.S. and S.L. Napelenok. 2011. "Air Quality Response Modeling for Decision Support". *Atmosphere* 2, 407–425. Available at <https://doi.org/10.3390/atmos2030407>.
- Dong, L., L.R. Leung, Y. Qian, Y. Zou, F. Song, and X. Chen. 2021. "Meteorological environments associated with California wildfires and their potential roles in wildfire changes during 1984-2017". *Geophys Res Atmos.* Available at <https://doi.org/10.1029/2020JD033180>.
- Emmons, L.K., S. Walters, P.G. Hess, J.-F. Lamarque, G.G. Pfister, D. Fillmore, C. Granier, A. Guenther, D. Kinnison, T. Laepple, J. Orlando, X. Tie, G. Tyndall, C. Wiedinmyer, S.L. Baughcum, and S. Kloster. 2010. "Description and evaluation of the Model for Ozone and Related chemical Tracers, version 4 (MOZART-4)". *Geoscientific Model Development* 3, 43–67. Available at <https://doi.org/10.5194/gmd-3-43-2010>.

- Goodkind, A.L., C.W. Tessum., J.S. Coggins, J.D. Hill, and J.D. Marshall. 2019. "InMAP Source-Receptor Matrix (ISRM) dataset (Version 1.2.1)". Zenodo. Available at <https://doi.org/10.5281/zenodo.3590127>.
- Grell, G.A., J. Dudhia, and D.R. Stauffer. 1994. *A description of the fifth-generation Penn State/NCAR mesoscale model (MM5)*. 128.
- Hakami, A., D.K. Henze, J.H. Seinfeld, K. Singh, A. Sandu, S. Kim, Byun, and Q. Li. 2007. "The Adjoint of CMAQ". *Environ. Sci. Technol.* 41, 7807–7817. Available at <https://doi.org/10.1021/es070944p>.
- Henze, D.K., A. Hakami, and J.H. Seinfeld. 2007. "Development of the adjoint of GEOS-Chem". *Atmospheric Chemistry and Physics* 7, 2413–2433. Available at <https://doi.org/10.5194/acp-7-2413-2007>.
- Heo, J. and P.J. Adams. 2015. *EASIUR User's Guide Version 0.2*.
- Heo, J., Adams, P.J., Gao, H.O. 2017. "Public health costs accounting of inorganic PM2.5 pollution in metropolitan areas of the United States using a risk-based source-receptor model". *Environment International* 106, 119–126. Available at <https://doi.org/10.1016/j.envint.2017.06.006>.
- Indeed. 2021. "Indeed - Waste Driver: Search Results". Available at <https://www.indeed.com/jobs?q=Waste+driver&l=California&radius=50>.
- Jin, L., N.J. Brown, R.A. Harley, J.-W. Bao, S.A. Michelson, and J.M. Wilczak. 2010. "Seasonal versus episodic performance evaluation for an Eulerian photochemical air quality model". *Journal of Geophysical Research* 115. Available at <https://doi.org/10.1029/2009JD012680>.
- Jin, L., R.A. Harley, and N.J. Brown. 2011a. "Ozone pollution regimes modeled for a summer season in California's San Joaquin Valley: A cluster analysis". *Atmospheric Environment* 45, 4707–4718. Available at <https://doi.org/10.1016/j.atmosenv.2011.04.064>.
- Jin, L., R.A. Harley, and N.J. Brown. 2011b. "Ozone pollution regimes modeled for a summer season in California's San Joaquin Valley: A cluster analysis". *Atmospheric Environment* 45, 4707–4718. Available at <https://doi.org/10.1016/j.atmosenv.2011.04.064>.
- Jin, L., A. Loisy, and N.J. Brown. 2013. "Role of meteorological processes in ozone responses to emission controls in California's San Joaquin Valley". *Journal of Geophysical Research: Atmospheres* 118, 8010–8022. Available at <https://doi.org/10.1002/jgrd.50559>.
- Jin, L., S. Tonse, D.S. Cohan, X. Mao, R.A. Harley, and N.J. Brown. 2008. "Sensitivity Analysis of Ozone Formation and Transport for a Central California Air Pollution Episode". *Environmental Science & Technology* 42, 3683–3689. Available at <https://doi.org/10.1021/es072069d>.
- Martien, P.T., R.A. Harley, and D.G. Cacuci. 2006. "Adjoint Sensitivity Analysis for a Three-Dimensional Photochemical Model: Implementation and Method Comparison". *Environ. Sci. Technol.* 40, 2663–2670. Available at <https://doi.org/10.1021/es0510257>.

- Muller, N.Z., and R. Mendelsohn. 2006. *The Air Pollution Emission Experiments and Policy Analysis Model (APEEP) Technical Appendix*.
- Napelenok, S., D.S. Cohan, Y. Hu, and A. Russell. 2006. "Decoupled direct 3D sensitivity analysis for particulate matter (DDM-3D/PM)". *Atmospheric Environment* 40, 6112–6121. Available at <https://doi.org/10.1016/j.atmosenv.2006.05.039>.
- Napelenok, S.L., D.S. Cohan, M.T. Odman, and S. Tonse. 2008. "Extension and evaluation of sensitivity analysis capabilities in a photochemical model". *Environmental Modelling & Software* 23, 994–999. Available at <https://doi.org/10.1016/j.envsoft.2007.11.004>.
- Nordahl, S.L., J.P. Devkota, J. Amirebrahimi, S.J. Smith, H.M. Breunig, C.V. Preble, A.J. Satchwell, L. Jin, N.J. Brown, T.W. Kirchstetter, and C.D. Scown. 2020. "Life-Cycle Greenhouse Gas Emissions and Human Health Trade-Offs of Organic Waste Management Strategies". *Environ. Sci. Technol.* 54, 9200–9209. Available at <https://doi.org/10.1021/acs.est.0c00364>.
- Paben, J. 2022. "California's diversion rate is now at 42%". *Resource Recycling*. January 18. Available at <https://resource-recycling.com/recycling/2022/01/18/californias-diversion-rate-is-now-at-42/>.
- Sandu, A., D.N. Daescu, G.R. Carmichael, and T. Chai. 2005. "Adjoint sensitivity analysis of regional air quality models". *Journal of Computational Physics* 204, 222–252. Available at <https://doi.org/10.1016/j.jcp.2004.10.011>.
- Scarborough, J., N. Clinton, and P. Gong. 2002. *Creating a Statewide Spatially and Temporally Allocated Agricultural Burning Emissions Inventory Using Consistent Emission Factors*. California Air Resources Board.
- Scown, C., A. Robinson, H. Breunig, L. Jin, T. Huntington, S. Smith, J. Devkota, S. Nordahl, N. Baral, and PepsiCo, Purchase, NY (United States). 2019. *Paths to Sustainable Distributed Generation through 2050: Matching Local Waste Biomass Resources with Grid, Industrial, and Community Needs* (No. LBNL--2001306, CEC--500-2019-XXX, 1616177). Available at <https://doi.org/10.2172/1616177>.
- SJVAPCD. 2016. *2016 Plan for the 2008 8-Hour Ozone Standard*. SJV Air Pollution Control District. Available at https://www.valleyair.org/Air_Quality_Plans/Ozone-Plan-2016.htm.
- Smith, S.J. 2020. *Designing the Organic Waste Management Sector in California: Understanding the Societally Optimal System, Private Sector Profitability, and the Impacts of Supportive policies (PhD dissertation)*. University of California, Berkeley.
- Tessum, C.W., J.D. Hill, and J.D. Marshall. 2017. *InMAP: A model for air pollution interventions*. PLoS ONE 12, e0176131. Available at <https://doi.org/10.1371/journal.pone.0176131>
- Thunis, P., B. Degraeuwe, E. Pisoni, F. Ferrari, and A. Clappier. 2016. "On the design and assessment of regional air quality plans: The SHERPA approach". *Journal of Environmental Management* 183, 952–958. Available at <https://doi.org/10.1016/j.jenvman.2016.09.049>.

- Trousdell, J.F., D. Caputi, J. Smoot, S.A. Conley, and I.C. Faloon. 2019. *Photochemical production of ozone and emissions of NO_x and CH₄ in the San Joaquin Valley*. *Atmos. Chem. Phys.* 19, 10697–10716. Available at <https://doi.org/10.5194/acp-19-10697-2019>.
- U.S. EPA. 2020. *User's Manual for the Co-Benefits Risk Assessment Health Impacts Screening and Mapping Tool (COBRA) Version 4.0*.
- U.S. EPA, 2018. *Technical Support Document EPA's 2014 National Air Toxics Assessment*.
- U.S. EPA, 2017. *Environmental Benefits Mapping and Analysis Program: Community Edition (BenMAP-CE) User Manual and Appendices*. Research Triangle Park, NC, USA.
- Van Dingenen, R., F. Dentener, M. Crippa, J. Leitaó, E. Marmer, S. Rao, E. Solazzo, and L. Valentini. 2018. "TM5-FASST: a global atmospheric source–receptor model for rapid impact analysis of emission changes on air quality and short-lived climate pollutants". *Atmos. Chem. Phys.* 18, 16173–16211. Available at <https://doi.org/10.5194/acp-18-16173-2018>.
- Wang, Y., L. Bastien, L. Jin, and R.A. Harley. 2023. "Location-Specific Control of Precursor Emissions to Mitigate Photochemical Air Pollution". *Environ. Sci. Technol.* 57, 9693–9701. Available at <https://doi.org/10.1021/acs.est.3c01934>
- Wang, Y., L. Bastien, L. Jin, and R.A. Harley. 2022. "Responses of Photochemical Air Pollution in California's San Joaquin Valley to Spatially and Temporally Resolved Changes in Precursor Emissions". *Environ. Sci. Technol.* 56, 7074–7082. Available at <https://doi.org/10.1021/acs.est.1c07011>
- WHO/Europe, 2020. *Health impact assessment of air pollution: introductory manual to AirQ+*.
- Zaman, A.U., 2013. "Life cycle assessment of pyrolysis–gasification as an emerging municipal solid waste treatment technology". *Int. J. Environ. Sci. Technol.* 10, 1029–1038. Available at <https://doi.org/10.1007/s13762-013-0230-3>.
- Zhao, Z., S.-H. Chen, M.J. Kleeman, and A. Mahmud. 2011a. "The Impact of Climate Change on Air Quality–Related Meteorological Conditions in California. Part II: Present versus Future Time Simulation Analysis". *Journal of Climate* 24, 3362–3376. Available at <https://doi.org/10.1175/2010JCLI3850.1>.
- Zhao, Z., S.-H. Chen, M.J. Kleeman, M. Tyree, and D. Cayan. 2011b. "The Impact of Climate Change on Air Quality–Related Meteorological Conditions in California. Part I: Present Time Simulation Analysis". *Journal of Climate* 24, 18.



**CALIFORNIA
ENERGY COMMISSION**



ENERGY RESEARCH AND DEVELOPMENT DIVISION

Appendix A: MODELING PROTOCOL

June 2024 | CEC-500-2024-066



APPENDIX A:

Modeling Protocol

The derivations of the adjoint method are detailed elsewhere (Bastien et al., 2015; Hakami et al., 2007; Henze et al., 2007; Martien et al., 2006; Sandu et al., 2005). In short, the user-specified quantity of interest (i.e., impact metric) is calculated from the concentrations output of chemistry-transport models (equation 1). For each particular choice of impact metric (by specifying g), there is a corresponding adjoint model (equation 2) that describes the evolution of the adjoint variable ψ (equation 3). This adjoint model should be numerically solved backward in time from a final condition. The change ∂R of impact metric to any change in model input can be calculated from ψ .

For each receptor and episode, one adjoint (backward) simulation can return a suite of adjoint sensitivities. These are sensitivities of the impact metric to adding/doubling emissions at each grid cell and each time step. Comparing to traditional forward sensitivities, the advantage of adjoint sensitivities is that the overall impacts (represented by changes in the impact metrics) are characterized, instead of only the local impacts. Outputs are resolved in space and time.

$$R = \int_0^T \iiint_0^\Omega g(C, x_1, x_2, x_3, t) dx_1 dx_2 dx_3 dt \quad (2)$$

$$\frac{\partial \psi}{\partial t} + u_i \frac{\partial \psi}{\partial x_i} = -\frac{\partial}{\partial x_i} \left(K_i \frac{\partial \psi}{\partial x_i} \right) - \frac{\partial g}{\partial C} \quad (3)$$

$$\psi = \frac{\partial g}{\partial C} \quad (4)$$

CMAQ_adj Model Configuration

The computer code used in this study is based on the adjoint of CMAQv4.5 by Hakami et al. 2007 with modification from Bastien et al., 2015. Bastien et al., 2015 used SAPRC99 chemical mechanism with ROSENBROCK chemical solver instead of the original CB-IV chemical mechanism used in Hakami et al. 2007. SAPRC99 includes 72 model chemical species and 211 chemical reactions (listed in Carter, 2000). Moreover, the original code is modified to force the time step for operator splitting (the synchronization time step, STS) to be constant throughout the simulation. Consequently, this time step is also used in the checkpointing time step. In the original code, the checkpointing time step is recalculated at each forward model run time step, based on the grid cell size and meteorological conditions. In this version of code (Bastien et al., 2015), the STS is calculated online at the beginning of the simulation as the minimum value that CMAQ would use for the current application. The same STS is used for the forward and the corresponding adjoint calculations but can vary across simulation periods. Additionally, CMAQv4.5 is configured to use the piecewise parabolic method for advection, multiscale horizontal diffusion, and eddy vertical diffusion (same as Jin et al. 2008 and 2010).

Photochemical Modeling Domain

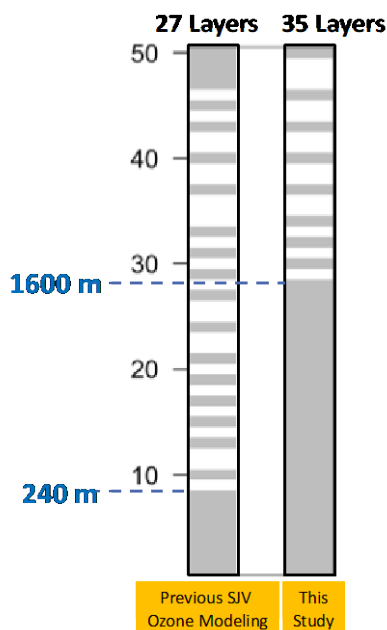
The study domain is a sub-region (34.5 to 39°N and 118.5 to 123°W) of the domain selected for the Central California Ozone Study, which consists of several geographically divided air basins including the SJV air basin and its major upwind source regions. The San Joaquin Valley is surrounded by the Sierra Nevada and coastal ranges. On typical summer days, westerly winds are funneled into the central valley through gaps in coastal ranges with large portions of the flow directed into SJV. Therefore, the San Francisco Bay area and Sacramento Valley are the major upwind SJV emission sources. Two busy highways run through the SJV: Highway 99 connects the major urban centers, and Interstate 5 runs through rural and agricultural areas. Air basins are labeled on the map for San Francisco Bay Area (SFB), Sacramento Valley (SV), Mountain County (MC), San Joaquin Valley (SJV), North and South Central Coast (NCC and SCC).

The study domain (hereinafter SARMAP domain) is modeled using a 96×117 grid with a horizontal resolution of 4 km. Vertically, the domain is divided into 35 layers from the surface to 100 mb (about 17 km); the near-surface layers are about 20 m thick.

Meteorological Inputs

Meteorological inputs are simulated by Wilczak and co-workers at NOAA (<http://www.etl.noaa.gov/programs/modeling/ccos/>) using the National Center for Atmospheric Research/Pennsylvania State University Mesoscale Meteorological Model Version 5 (MM5) (Grell et al. 1994) version 3 for a historical summer season starting at 1200 UTC June 1 to 1200 UTC September 30, 2000. Meteorological fields with 4 km resolution were used as input for air quality modeling in this study. The Meteorology to Chemistry Interface Processor (MCIP version 3.6) was used to construct CMAQ model-ready input files from the MM5 output, and it allows for consolidation of vertical layers. We used 35 layers for CMAQ from the original 50 MM5 layers without changing the first 1600 m (28 layers) to preserve high resolution within the planetary boundary layer (PBL) Note that this vertical layer collapsing choice is different from the one used in previous CMAQ modeling study conducted in this domain (Jin et al., 2011b, 2010, 2008) (Figure A-1).

Figure A-1: Vertical Layer Collapsing Used In This Study



Three ozone episodes are extracted for ensemble simulations to understand variation of influential source regions with meteorological conditions (previously shown in Table 1 and Figure 3). These episodes were statistically identified in previous studies to capture representative temperature and flow regimes in a historical summer season in the SJV modeling domain (Jin et al., 2013, 2011b). Each episode is named after the region where O₃ concentrations are high during the period: O₃-North, O₃-South, O₃-West, and O₃-All (Jin et al 2013, Figure 3). For example, from July 29 to August 2, O₃ is high throughout the valley or from June 21 to 25, O₃ is high in the north side of the valley. These O₃ episodes are extended to 7-day modeling periods, which include a 4-day model spin-up at the beginning of each period.

Emission Inputs

Ozone sensitivity to emissions vary with not only meteorology but also the baseline emissions (Jin et al. 2013) that change from year to year due to emission controls. In order to capture the most recent chemical environment for ozone formation, we obtained hourly gridded emission inputs of the gaseous species derived from the 2012 emission inventory for the most recent SJV Ozone State Implementation Plan (SJVAPCD, 2016) prepared by California Air Resources Board (CARB).

The gridded emissions are provided in two types of files: one is the merged emissions including anthropogenic (point, area, and mobile sources) and biogenic sources, the other is the biogenic emissions only. The SARMAP domain (96 by 117) is contained within the CARB domain (192 by 192) with the same horizontal resolution and map projection. The anthropogenic portion of the CARB emission data is originally speciated under the SAPRC07 chemical mechanism (Carter, 2010b) and is mapped to the SAPRC99 speciation (Carter, 2000) required for CMAQ v4.5 according to Table A-1.

Table A-1: Species Mapping from SAPRC07 to SAPRC99 (same species are omitted)

Name in SAPRC07	Description in SAPRC07	Name in SAPRC99	Description in SAPRC99, if different
AACD	Acetic Acid. Also used for peroxyacetic acid.	CCO_OH	Acetic Acid
ACRO	acrolein	METHACRO	methacrolein and acrolein
ACYE	acetylene	ALK2	Alkanes and other non-aromatic compounds that react only with OH and have kOH between 5×10^2 and $2.5 \times 10^3 \text{ppm}^{-1} \text{min}^{-1}$. (Primarily propane and acetylene)
APIN	a-Pinene	TRP1	terpenes
B124	1,2,4-Trimethylbenzene	ARO2	Aromatics with kOH $> 1.4 \times 10^{-11} \text{cm}^3/\text{molec}/\text{sec}$
BDE13	1,3-Butadiene	OLE2	Alkenes with kOH $> 4.8 \times 10^{-11} \text{cm}^3/\text{molec}/\text{sec}$
BENZ	Benzene	ARO1 (weighted by 0.3)	Aromatics with kOH $< 2 \times 10^4 \text{ppm}^{-1} \text{min}^{-1}$.
CRES	Phenols and Cresols	CRES	Cresols
ETHE	ethene	ETHENE	
ETOH	Ethanol	ALK3	
FACD	Formic Acid	HCOOH	
IPRD	Unsaturated aldehydes with internal double bonds. Based on C5 isoprene product species.		
ISOP	Isoprene	ISOPRENE	
MACR	Unsaturated aldehydes with terminal double bonds. Based on methacrolein.	METHACRO	Methacrolein
MVK	Unsaturated ketones (based on methyl vinyl ketone).	MVK	Methyl Vinyl Ketone
MXYL	m-Xylene	ARO2	Aromatics with kOH $> 1.4 \times 10^{-11} \text{cm}^3/\text{molec}/\text{sec}$
OXYL	o-Xylene	ARO2	
PACD	Higher organic acids and peroxy acids (mechanism based on propionic acid).	RCO_OH	higher organic acids

Name in SAPRC07	Description in SAPRC07	Name in SAPRC99	Description in SAPRC99, if different
PRD2	Ketones and other non-aldehyde oxygenated products which react with OH radicals faster than $5 \times 10^{-12} \text{cm}^3/\text{molec}/\text{sec}$.	PROD2	
PRPE	Propene	OLE1	Alkenes other than ethene with $k_{OH} < 4.8 \cdot 10^{-11} \text{cm}^3/\text{molec}/\text{sec}$ (primarily terminal alkenes)
PXYL	p-Xylene	ARO2	Aromatics with $k_{OH} > 1.4 \times 10^{-11} \text{cm}^3/\text{molec}/\text{sec}$
TERP	Terpenes	TRP1	
TOLU	Toluene	ARO1	Aromatics with $k_{OH} > 1.4 \times 10^{-11} \text{cm}^3/\text{molec}/\text{sec}$

Note that the purpose of this project is not to reproduce day to day ozone concentrations of summer 2012, but to understand how source-receptor relationships vary with meteorology (including direct meteorology effects such as flow pattern, effects on reaction rates, and indirect effects on biogenic emissions). Two sets of anthropogenic emissions are prepared. The first set of emissions representing the weekdays' emissions is constructed with Wednesday emissions of O₃-All episodes. Those emissions were found to be most similar to weekday emissions averages. The second set of emissions representing the weekend's emissions is constructed with Sunday emissions from O₃-All episodes. Sunday's emissions were chosen because they are lower than Saturday and will give us the largest difference between weekend and weekday in order to see the upper bound of difference. As the year 2000 meteorological inputs are used to drive the chemical transport model and variations in biogenic emissions are largely driven by light and temperature fields, the two sets of anthropogenic emissions are merged with the meteorological driven biogenic emissions of year 2000 (documented in Jin et al. 2010).

Lateral Chemical Boundary and Initial Condition

The initial chemical conditions (ICON) define the mixing ratios of gaseous species in the modeling domain at the beginning of the model simulation. Lateral chemical boundary conditions (BCON) define the chemical species mixing ratio at the four boundaries at where the air enters or leaves the modeling domain. A four-day spin-up run prior to each episode is used to obtain the model initial conditions.

Vertically varying boundary conditions are provided by CARB at hourly resolution. CARB BCON was derived from the global simulations using the Model for Ozone And Related chemical Tracers (MOZART) (Emmons et al., 2010) version 4. As the CARB BCON is speciated under the

SAPRC07 chemical mechanisms, mapping to the SAPRC99 mechanism is conducted similarly according to Table A-1.

The western boundary represents an inflow boundary at which the chemical species enter the domain and interact with the chemical transport processes. The other three boundaries largely represent outflows and therefore have less impacts on the ozone formation and transport within the domain (see diagnostics in Jin et al. 2008 and 2010). The temporally average concentrations of the CARB BCON at each of the four boundaries over the four-episode time periods are used to represent the chemical environment at the lateral boundaries surrounding the domain. Selected species at the western boundary are showing at various heights in Table A-2.

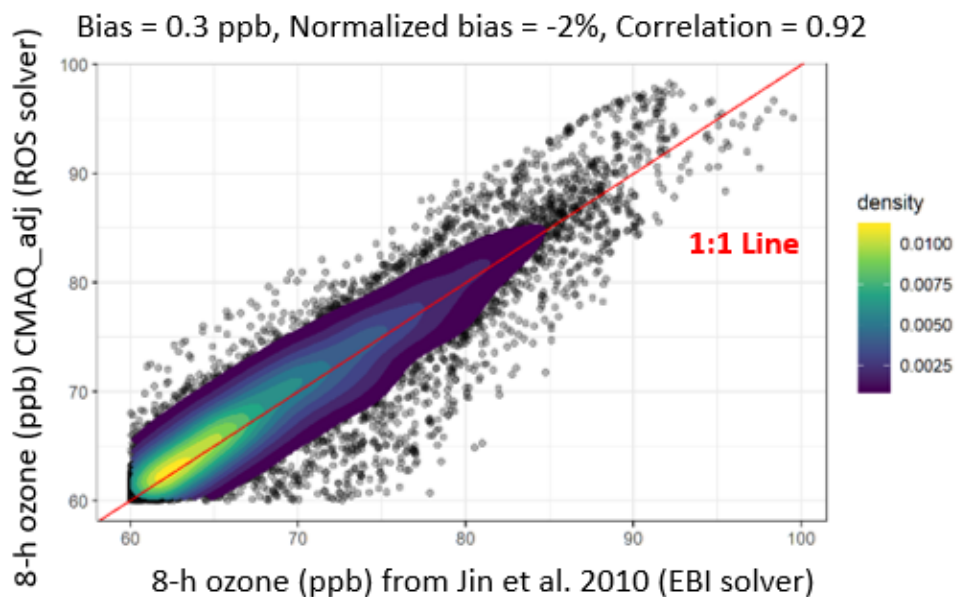
Table A-2: Vertical variation of western BCON for selected species (ppb)

Height (m)	NO₂	NO	O₃	CO	PAN
surface	0.08	0.01	25	103	0.04
300	0.06	0.01	25	102	0.04
800	0.04	0.01	38	101	0.02
1000	0.04	0.01	40	100	0.02
3000	0.05	0.01	47	90	0.08
8000	0.03	0.01	57	86	0.21
13000	0.04	0.02	90	79	0.27
16000	0.12	0.09	194	54	0.17

Forward Model Evaluation

The adjoint code is coupled to CMAQ (v4.5) and configured with the same build options as the stand-alone CMAQ4.5, including chemical mechanisms, advection and diffusion schemes, horizontal and vertical resolutions. The stand-alone CMAQ v4.5 has been benchmarked in previous studies in the central California domain by comparing predicted concentrations to observed values and showed steady and adequate performance over the ozone season (Jun to Sep) and for individual ozone episodes (Jin et al. 2008, 2010). The chemical solvers used are slightly different: stand-alone CMAQ4.5 used EBI solver and CMAQ_adj uses Rosenbrock solver. A 5-day forward simulation of CMAQ_adj is conducted from July date 206 to 211. The forward simulation is evaluated by comparing simulated 8-h peak ozone against the previously benchmarked simulations in Jin et al. 2008 (Table A-2) for the same domain. The comparison shows small (2% on average) difference and good correlation 0.92.

Figure A-2: Comparison between forward CMAQ_adj and benchmark.



Adjoint Sensitivity Evaluation

The accuracy of the adjoint model is evaluated by comparing adjoint sensitivities with sensitivities obtained by brute-force (BF) method. Due to computational costs, the adjoint sensitivity is evaluated for a smaller domain within the SJV domain indicated by the grey rectangle in Figure A-3. The receptor regions: FSF_DAY, RUR_DAY, and RUR_BDAY labeled in Figure A-3, are chosen to cover various urban and rural receptor locations in the evaluation domain. BF sensitivities are calculated by perturbing emissions at a single grid cell by adding a constant value throughout a 24-hour period. This constant value is chosen as roughly 10% of the maximum emissions of a given species observed in the perturbation domain (orange rectangle in Figure A-3) upwind of the receptor regions. Twenty grid cells are evenly chosen in the perturbed domain for the perturbation. The perturbation amplitudes of 0.1 mol/sec, 0.005 mol/sec, 0.015 mol/sec, 0.01 mol/sec, 0.03 mol/sec of NO, HCHO, OLE1, ARO1, ETHENE, respectively, are hourly added to each of twenty 4km × 4km grid cells. The simulation is conducted for a 1-day period. As a result, there are 300 (= 20 perturbed grid cells × 3 receptors × 5 perturbed species) data points that can be compared.

The receptor (or model response) is defined as average O₃ concentrations from 10 am to 5 pm local time over the receptor region. The response is mathematically described as:

$$R = \int_0^T \iint_{\Omega_S} P_{\Omega_S}(x_1, x_2, t) C(x_1, x_2, t) dx_1 dx_2 dt \quad (8)$$

where R is the model response, Ω_S is the modeling domain, P_{Ω_S} is the weighting factor for the location and time, C is the concentrations output, T is modeling period, and x_1, x_2 are the coordinate of the domain.

For the BF approach, each perturbed emissions point requires a single forward run with perturbed input at that point to obtain one response. The responses from the perturbed cases

are then compared to the non-perturbed cases to obtain the BF sensitivities. The BF sensitivities are calculated by:

$$S_{E_i}^{BF} = \frac{\Delta R}{\Delta E_i} = \frac{R_{perturbed} - R_{non_perturbed}}{\Delta E_i} \quad (9)$$

where ΔE_i is the added emissions, $R_{perturbed}$, $R_{non_perturbed}$ are the response with perturbed input and non-perturbed input, respectively.

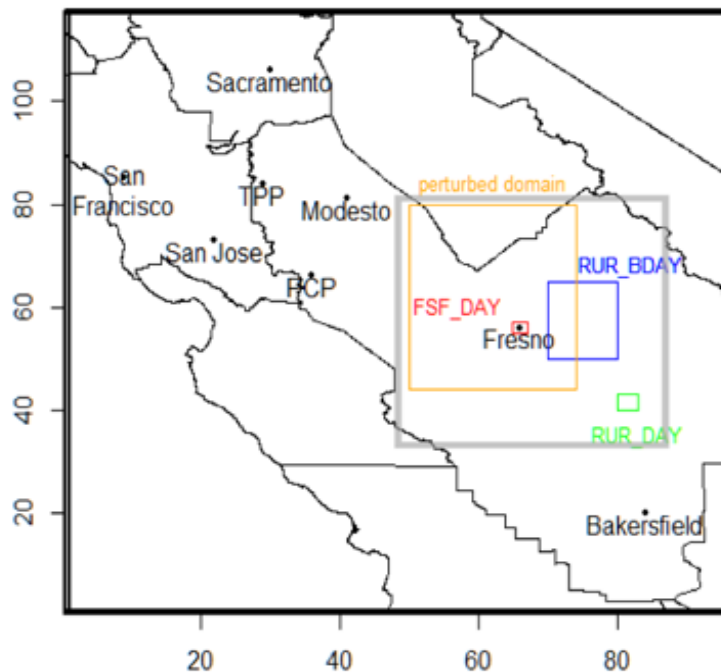
The relative changes in model response calculated by the BF method and adjoint method are plotted in Figure A-4:

$$\%BF = \frac{\Delta R}{R_{non_perturbed}} = \frac{S_{E_i}^{BF} \times \Delta E_i}{R_{non_perturbed}} \times 100\% \quad (10)$$

$$\%adjoint = \frac{\Delta R}{R_{non_perturbed}} = \frac{S_{E_i}^{adj} \times \Delta E_i}{R_{non_perturbed}} \times 100\% \quad (11)$$

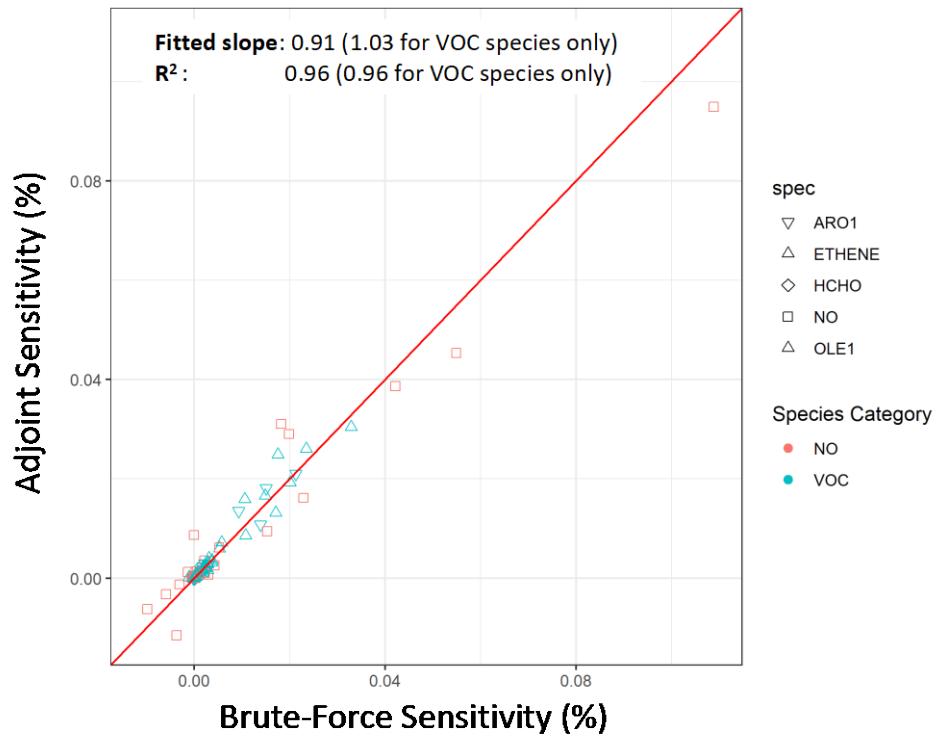
where $S_{E_i}^{BF}$, $S_{E_i}^{adj}$ are the additive sensitivities obtained from BF method and adjoint method, respectively.

Figure A-3: Receptor regions and perturbed emissions domain. Gray rectangle indicates the evaluation subdomain.



Adjoint and BF show good agreement for perturbations in NO (red points) and VOCs (blue points) with a coefficient of determination $R^2=0.96$ (Figure A-4). The correlation is about the same if only VOCs are concerned ($R^2=0.96$). Such performance behavior is consistent with previous adjoint evaluation conducted for the San Francisco Bay Area domain using the same code (Bastien et al. 2019).

Figure A-4: Relative change in the model response obtained by first-order adjoint sensitivities compared to BF sensitivities method.





**CALIFORNIA
ENERGY COMMISSION**



ENERGY RESEARCH AND DEVELOPMENT DIVISION

Appendix B: EMISSION FACTORS

June 2024 | CEC-500-2024-066



APPENDIX B:

Emission Factors

Table B-1: Emission Factors Used in the Case Study

Process	Waste Type	NO _x	VOC	Unit	Sources and Assumptions
Transportation	All	0.1369889	0.00856181	g/(km-tonne)	EMFAC2007, Flatbed trucks are used for the pickup and delivery of waste biomass
Agricultural residue burning	Alfalfa	2.25	10.85	kg/wet tonne	CARB report of "Creating a Statewide Spatially and Temporally Allocated Agricultural Burning Emission Inventory Using Consistent Emission Factors" (Scarborough et al., 2002)
	corn	1.65	3.3	kg/wet tonne	
	sorghum	2.25	2.55	kg/wet tonne	
	rice	2.6	2.35	kg/wet tonne	
	safflower	2.25	7.4	kg/wet tonne	
	wheat	2.15	3.8	kg/wet tonne	
	almonds	2.95	2.6	kg/wet tonne	
	apples	2.6	1.15	kg/wet tonne	
	apricots	2.6	2.3	kg/wet tonne	
	plums	2.6	2.3	kg/wet tonne	
	Avocado	2.6	9.25	kg/wet tonne	
	dry_beans	2.6	7.1	kg/wet tonne	
	cherries	2.6	3	kg/wet tonne	
	citrus_other	2.6	3.4	kg/wet tonne	
	Date Palm	2.6	1.9	kg/wet tonne	
grapes	2.6	1.9	kg/wet tonne		

Process	Waste Type	NO_x	VOC	Unit	Sources and Assumptions
	nectarines	2.6	1.15	kg/wet tonne	
	peaches	2.6	1.5	kg/wet tonne	
	olives	2.6	5.15	kg/wet tonne	
	pears	2.6	2.55	kg/wet tonne	
	walnuts	2.25	2.4	kg/wet tonne	
	barley	2.55	7.5	kg/wet tonne	
	oats	2.25	5.15	kg/wet tonne	
	Fig	2.6	3	kg/wet tonne	
	orchard	2.6	3.15	kg/wet tonne	

Emission factors of other processes are estimated using the methodology and data sources as documented in a previous publication (Nordahl et al., 2020).